NTNU
Norwegian University of
Science and Technology

Analysis and Design of Floating Bridge over Bjørnefjorden

Floating Bridge Subjected to Large Ship Collisions

Ole Eldegard

Marine Technology
Submission date: February 2017
Supervisor: Jørgen Amdahl, IMT

Norwegian University of Science and Technology
Department of Marine Technology

NTNU – Trondheim
Norwegian University of
Science and Technology

Analysis and Design of Floating Bridge over Bjørnefjorden

Floating Bridge Subjected to Large Ship Collisions

Ole Eldegard

February 2017

Master Thesis
Department of Marine Technology
Norwegian University of Science and Technology

Supervisor: Prof. Jørgen Amdahl
Co-supervisor: Post. doc Yanyan Sha

NTNU
Norges teknisk-naturvitenskapelige universitet
Institutt for marin teknikk

MASTER THESIS 2016

For

Stud. Techn. Ole Eldegard

Analysis and Design Bjørnefjorden Floating Bridge Subjected to Large Ship Collisions

Analyse og dimensjonering Bjørnefjorden flytebro utsatt for støt fra store skip

The Norwegian Public Roads Administration (NPRA) is running a project "Ferry free coastal route E39", where suspension bridges, floating bridges or submerged tunnels would be installed across fjords in Western Norway. The straits are up 5 kilometres wide and will call for significant extension of present technology. Several innovative crossing concepts have been proposed. One of them is the combined floating-cable bridge concept.

The bridge has to resist extreme environmental loads and accidental actions with acceptable safety levels. One of the concerns are accidental ship collisions with energies 100-1500 MJ. The proposed concepts cannot be designed adequately using existing methods and design rules. Consequently, advanced scenario-based analyses have to be conducted based on accurate simulation of the governing physical processes.

For crossing of Bjørnefjorden one of the most relevant concept is floating bridge with a cable stayed section in the south end.

The purpose of the work is to perform scenario-based and advanced analysis of ship collision with the bridge and to assess the response of the bridge exposed to extreme environmental loads, both in intact and damaged condition.

In the project work a finite element model with the navigation channel in the middle of the fjord was developed. At present, the most relevant location of the navigation channel is in the south end, hence an existing finite model of this solution will be provided. .

Scope of work:

1. Critical review of the finite model of the bridge used for USFOS analysis. Improve model to the extent needed. Conduct eigenvalue analysis.

2. An existing model of the bridge girder including a local shell finite element model in the collision-exposed area used for LS-DYNA analysis will be made available. Perform a critical review of the model and modify the model as deemed necessary. This model shall be used in integrated collision analysis. Finite element models of ship bows (container vessel, large passenger vessel, Ro-Ro ship) will be made available. Of particular interest are the collision force-time- and collision force-deformation relationships as well as local damage to the bridge girder. The damage obtained in integrated LS-DYNA analysis shall be transferred to the USFOS model as far as possible.

3. Conduct dynamic, time domain simulation of ship collision with the bridge. Updated ship force-deformation curve obtained from LS-DYNA analysis shall be modelled using the nonlinear spring concept. The ship shall be represented by a nodal mass with initial velocity. Central collisions shall be assumed initially.

4. Perform analysis of non-central impacts, with the pontoons where ship may be deflected away from the pontoon. Use a new model for global ship motions provided that the model becomes available during thesis period.

5. Conduct residual strength analysis of the bridge with collisions damage exposed to extreme environmental loads.

6. Conduct analysis of the bridge subjected to extreme environmental loads using the contour line method applied to offshore structures. Analysis shall be carried out with both static and stochastic wind loads, the latter using the WINDSIM software. Include relevant wave loads. Slowly varying drift forces and sum frequency forces shall be considered.

7. Conclusions and recommendations for further work

Literature studies of specific topics relevant to the thesis work may be included.

The work scope may prove to be larger than initially anticipated. Subject to approval from the supervisor, topics may be deleted from the list above or reduced in extent.

In the thesis the candidate shall present his personal contribution to the resolution of problems within the scope of the thesis work.

Theories and conclusions should be based on mathematical derivations and/or logic reasoning identifying the various steps in the deduction.

The candidate should utilise the existing possibilities for obtaining relevant literature.

The thesis should be organised in a rational manner to give a clear exposition of results, assessments, and conclusions. The text should be brief and to the point, with a clear language. Telegraphic language should be avoided.

The thesis shall contain the following elements: A text defining the scope, preface, list of contents, summary, main body of thesis, conclusions with recommendations for further work, list of symbols and acronyms, references and (optional) appendices. All figures, tables and equations shall be numerated.

The supervisor may require that the candidate, in an early stage of the work, presents a written plan for the completion of the work. The plan should include a budget for the use of computer and laboratory resources, which will be charged to the department. Overruns shall be reported to the supervisor.

The original contribution of the candidate and material taken from other sources shall be clearly defined. Work from other sources shall be properly referenced using an acknowledged referencing system.

The report shall be submitted in two copies:

- Signed by the candidate
- The text defining the scope included
- In bound volume(s)
- Drawings and/or computer prints which cannot be bound should be organised in a separate folder.

Supervisor NTNU:
Prof. Jørgen Amdahl

Co-supervisor:
Postdoc Yanyan Sha

Deadline: February 2, 2017

Trondheim, August 20, 2016

Jørgen Amdahl

Preface

This Master's Thesis is the result of the work done by stud. techn. Ole Eldegard at the Norwegian University of Science and Technology during the fall of 2016. The scope of work was developed by Professor Jørgen Amdahl and builds on the Project Thesis written during the spring of 2016.

Point 1 in the scope of work was meant to include only a brief assessment of an USFOS model for the bridge, developed by Post. Doc. Yanyan Sha, which should be used for the analyses in this Thesis. This task proved to be much more time consuming than first anticipated. At the time of starting the work with the Master's Thesis, the model was only a first suggestion, where many of the parameters were meant to be improved at a later stage. Due to a minor miss-communication, Supervisor Jørgen Amdahl was of the impression that the model was more or less ready for running the collision analyses.

Additionally, the information given for the bridge, through bridge drawings and a project report were incomplete, and large parts of the bridges dimensions had to be calculated based on assumptions, and the limited data available. As more parameters were set, it was possible to cross check many of the parameters by relating them to other properties through more calculations. This was thus much more time consuming than modeling the bridge directly from complete drawings, and several errors, which had to be corrected were made during this work.

The USFOS model used in the analyses utilized some commands, that had no available documentation. This proved to cause some trouble during the modeling, due to misinterpretation as to how the commands should be implemented in the USFOS code, and of what exactly the commands introduced to the model. Especially the buoyancy elements caused the analysis to fail repeatedly.

As explained, task 1 of the scope of work, proved to introduce a much larger workload than first anticipated. Because of this, task 5 and 6 were not finished. In agreement with supervisor Professor Jørgen Amdahl, it was thus decided that it was more important to get accurate results for point 3, which was the most important part of the work. Most of the extra work related to point 1 are not presented in this Thesis, to keep it concise and to the point. Only the information deemed essential for the results is included, and the work presented in this thesis thus do not reflect the workload correctly.

Point 5 and 6 in the scope of work were initially meant as suggestions for extra work, should the rest of the task be easily overcome. Point 4 on the list could only be done provided that the model for non-central impacts in USFOS was developed in time. This was not the case, and this work could thus not be done.

To introduce the ship collision force into the model, the results from a local bow crushing analysis was used. This analysis was performed by Post. Doc Yanyan Sha on a model developed by Ole Harald Moe. The work was also delayed further when waiting for the results from this analysis.

I would like to thank Supervisor Professor Jørgen Amdahl for the support he has given through guidance during this thesis. Due to the lack of documentation available on certain parts of the software used, guidance was needed on details in the analyses, and he made himself available whenever needed. The help from Post. Doc Yanyan Sha was also crucial for the work done in this thesis. Especially during the development of the USFOS model. I feel that it is necessary to clarify that, despite errors in the initial model being mentioned throughout this Thesis, this

do not indicate that the modeling work done by Yanyan Sha was flawed. The model was only intended as an initial suggestion for a model.

I would also thank Tore Holmås for valuable insight when setting up the USFOS analysis, and Kirsti Skogseth for developing the illustration used on the cover of this Thesis.

Because the model is based on information that is private property, Presentation of the model's details, are kept to a minimum, and some of the details have been censored. The USFOS code will not be published, to prevent the work from plagiarism, and for more information, or for further use of the model, one would have to contact the author of this thesis.

Abstract

In This Master's Thesis, a bridge design for the crossing of Bjørnafjorden have been investigated. The design was developed in a cooperation between COWI, Aas Jakobsen, Johs Holte As and Global Maritime, as a part of The Norwegian Public Roads Administrations (NPRA) project "ferry free E39". The project is still in the early stages, where the feasibility of different bridge designs are being evaluated. The design analysed in this project is a curved floating bridge, with a cable-stayed section near land in the south end, to allow for ship traffic to pass under the bridge. It is floating freely without moorings, and the curved design help tocarry shear forces through membrane stresses.

The bridges global strength against ship collisions have been investigated throughout this Thesis. Theoretical background is presented initially, before different analyses are conducted in the software USFOS. An initial suggestion of a bridge model used in the USFOS analyses, were developed by Post. doc Yanyan Sha. During the work with this Master's Thesis, this much time were spent to improve this model, for the analyses to give realistic results, despite the significant number of uncertainties being present in this early stages of the project.

An eigenvalue analysis was conducted, and large period deflection modes were observed for horizontal bending of the bridge girder. The maximum eigenvalue was found to be 62.66 seconds. The results of the eigenvalue analysis were compared with the results obtained by COWI et al., through the software Orcaflex, and were found to correspond well. This gave gave confidence for the mode being able to represent thes structural response of the bridge fairly well.

No information were obtained for the damping level of the bridge, and to reduce the uncertainties this would introduce for the final results, a separate damping assessment where performed. An analysis, where the pontoon closest to the navigational channel, was exposed to a ship impact with collision energy of 1250 MJ, was run several times with different damping levels. By comparing the results from these analyses, it was found that even for large changes in the level of damping introduced to the model, the change in the final results were only in the order of a few percent. This is most likely because the most critical response occur shortly after impact, and little energy have had the time to be lost to damping.

In the main ship collision analysis three different collision scenarios were investigated, and due to uncertainties with respect to the what collision energies the bridge should be designed against, a range of different collision energies were introduced. In Collision scenario 1, the ship hits the short end of the pontoon closest to the navigational channel. The maximum collision energy of 900 MJ, gives a maximum plastic utilization factor of 0.905, occurring third crossbeam to the north of the struck pontoon. Due to difficulties in modeling the pre-tension in the wires of the cable stayed section, false stresses occur due to the permanent loads of the bridge. Because of this, the value of the plastic utilization is not not used for the bridge girder of this part of the bridge. Instead, the increase in the plastic utilization is found. For the maximum collision energy, the increase in the plastic utilization is found to have a maximum value of 0.486, in the girder above the connection to the column of the struck pontoon. From this it is concluded that the bridge will survive the impact, as long as the plastic utilization factor due to the permanent loads do not exceed 0.5.

From the analyses of collision scenario 2, where the pontoon closest to the navigational channel is struck in the transverse direction, very high plastic utilization factors were observed in the

column of the struck pontoon. At the top of the column, in the connection to the bridge girder, the plastic utilization factor was found to be 0.992 for the lowest collision energy investigated of 500 MJ. For the maximum collision energy of 900 MJ, large plastic deformations are observed, and it is thus advised to strengthen the upper part of the pontoon columns.

In collision scenario 3, the plastic utilization factors observed, are low, with a maximum value of 0.763 in one of the cross beams. The global strength of the bridge thus seem to be sufficient for collision like this, into the bridge girder, and no strengthening are advised. The collision energies used for this collision scenario are much lower than for collision scenario one and two, with a maximum value of 450 MJ. This is a result of it being further away from the navigational channel, and thus was found to be less prone to collisions in the analysis performed by the SSPA.

Norsk sammendrag

I denne Masteroppgaven har et brodesign for kryssing av Bjørnafjorden blitt analysert. Brodesignet ble utviklet i et samarbeid mellom COWI, Aas Jakobsen, Johs Holte As og Global Maritime, som en del av Statens Vegvesens prosjekt "ferjefri E39". Prosjektet er fortsatt i en tidlig fase, hvor gjennomførbarheten til forskjellige brodesign blir avdekket. I denne oppgaven undersøkes en buet flytebro, hvor skipsleden går under en strekkstagsbro nær land i sørenden av broen. Broen flyter fritt uten ankerliner, og det buede designet bidrar til å bære skjærkrefter på broen ved membrankrefter.

Broens globale styrke mot skipsstøt er undersøkt, gjennom arbeidet med denne Masteroppgaven. Det teoretiske grunnlaget for undersøkelsene presenteres, før forskjellige analyser utføres i programvaren USFOS. Et førsteutkast for bromodellen brukt i analysene ble utviklet av Post. doc Yanyan Sha, og omfattende arbeid ble lagt ned for å videreutvikle denne modellen.

Gjennom å gjennomføre en egenverdianalyse ble de viktigste egenfrekvensene og modene til broen avdekket. Den største egenperioden til broen ble funnet med en periode på 62.66 sekunder. Resultatene fra egenverdianalysen ble kontrollert ved å sammenlikne resultatene med resultatene fra egenverdianalysene gjort av COWI m.fl. i programvaren Orcaflex. Resultatene samsvarte godt, og det kan derfor forventes at fysikken til brodesignet er nok så godt modellert av USFOS modellen brukt.

Ingen informasjon var tilgjengelig for hvor stor dempning broen vil oppleve, og for å redusere usikkerheten rundt resultatene som dette vil medføre, ble det gjennomført en separat undersøkelse av broens demping. En analyse av et skipsstøt med kollisjonsenergi på 1250 MJ, mot kortsiden av pongtongen nærmest skipsleden, ble gjennomført for forskjellig grad av dempning. Resultatet fra analysen ble sammenlignet for de forskjellige dempningsgradene for å se effekten dempingen hadde på sluttresultatet av analysene. Det ble avdekket at selv ved stor variasjon i graden av demping, så hadde sluttresultatet en relativ endring på kun et par prosent. Dette skyldes mest sannsynlig at den mest kritiske responsen oppstår kort tid etter kollisjonen, og lite energi rekker derfor å gå tapt til dempning.

I hovedanalysen gjort på skipsstøt, er tre forskjellige kollisionsscenarier undersøkt. Siden stor usikkerhet er knyttet til hvilke kollisjonsenergier broen må dimensjoneres mot, er analysene kjørt med en rekke forskjellige kollisjonsenergier. I kollisjonsscenario 1, kolliderer skipet med kort-enden av pongtongen nærmest skipsleden. For den største kollisjonenergien, på 900 MJ, blir den maksimale plastiske utnyttelsesfaktoren 0.905, og er observert i den tredje tverrbjelken nord for pongtongen.

Siden forspenningen i strekkstagene ikke kan modelleres korrekt i programvaren benyttet, oppstår det falske spenninger i brobjelken nær strekkstagene, når vekten av broen introduseres. På grunn av dette kan ikke den plastiske utnyttelsesfaktoren benyttes for å vurdere påkjenningen til broen, siden den allerede er svært høy fra vekten av broen. Isteden må økningen i den plastiske utnyttlesesfaktoren undersøkes. For den høyeste kollisjonsenergien blir en økning på 0.486 i den plastiske utnyttelsesfaktoren observert. Fra dette kan det konkluderes med at så lenge den plastiske utnyttelsen grunnet vekten av broen er på mindre 0.5, så vil ikke broen trenge utbredelser.

I kollisjonsscenario 2 blir den samme pongtongen truffet på langsiden, og resultatene fra analysene avdekker en veldig høy plastisk utnyttelse av søylene til pongtongen som er truffet. På toppen av søylene, nær festet til brobjelken, blir det observert en plastisk utnyttelsesfaktor på

hele 0.992 for den laveste kollisjonsenergien. For den høyeste kollisjonsenergien blir det observert store plastiske deformasjoner, og det er derfor anbefalt å forsterke den øverste delen av disse søylene.

I det tredje kollisjonsscenariet blir det funnet at de plastiske utnyttelsesfaktorene er lave, og den største verdien er på 0.763, observert i en av tverrbjelkene. Den globale styrken til broen ser ut til å være stor nok for denne typen påkjenning, og ingen forbedringer ser ut til å være nødvendig. Kollisjonsenergiene benyttet for dette kollisjonsscenariet er mye lavere, enn for de to andre analysene, med en maksimumsenergi på 450 MJ. Dette er med bakgrunn i at denne delen av broen ligger lenger vekk fra skipsleden, og ble derfor funnet å være mindre utsatt for skipsstøt.

Table of Contents

List of Figures

List of Tables

Nomenclature

Abbreviations

AIS	Automatic identification system
ALS	Accidental limit state
$HHT-\alpha$	Hilbert-Hughes-Taylor-α
$NPRA$	Norwegian Public Roads Administration
$Post.doc$	Postdoctoral researcher
$Prof.$	Professor
ULS	Ultimate limit state

Greek Symbols

α_1	Parameter in Rayleigh distribution
α_2	Parameter in Rayleigh distribution
β	Parameter of Newmark-β method
δ	Reduction in crushing depth
γ	Parameter of Newmark-β method
λ	Damping ratio
$\lambda(x)$	Probability of failure per traveling distance
ϕ	Mode shape
∇	Displacement
ω	Angular frequency
ρ	Density

Latin Symbols

$\ddot{\mathbf{q}}$	Nodal accelerations
$\ddot{\mathbf{r}}$	Nodal accelerations

$\dot{\mathbf{q}}$	Nodal velocities
$\mathbf{C}$	Damping matrix
$\mathbf{F}$	Force vector
$\mathbf{K}$	Stiffness matrix
$\mathbf{M}$	Mass matrix
$\mathbf{Q}$	Load vector
$\mathbf{q}$	Nodal displacements
$\mathbf{r}$	Nodal displacements
$\tilde{t}$	Alternative defenition of time used in the HHT-α method
C_D	Drag coefficient
C_{diff}	Diffraction coefficient
C_{drag}	Drag coefficient
D	Diameter
$f_s(y)$	Distribution of initial ship position
F_{diff}	Diffraction damping force
F_{drag}	Drag force
g	Gravitational constant
h	1. Height of submerged body 2. Step length of iterations
I_t	Polar moment of inertia
I_x	Moment of inertia about the x-axis
I_z	Moment of inertia bout the z-axis
k	Stiffness of the ship
m	Mass of ship
n	Number of ships per time unit
P_a	The probability that a collision is avoided by human intervention
$P_c(x, y)$	Conditional probability of collision, given initial position
r	Rounding radius
T	Period

t Time

u Water speed

$v(x, y)$ Impact velocity if ship, given starting position

W_{ey} Elastic shear modulus about the y-axis

W_{ez} Elastic shear modulus about the z-axis

W_{pt} Plastic torsional modulus

W_{px} Plastic shear modulus about the x-axis

W_{pz} Plastic shear modulus about the z-axis

Chapter 1

Introduction

This project Thesis will be looking at a bridge design for the crossing of Bjørnafjorden on the west coast of Norway. The fjord crossing is part of The Norwegian Public Roads Administrations (NPRA) project ”ferry free E39”. The goal is to improve the quality of E39 between Kristiansand and Trondheim, to promote growth in trade and business in the region. To reduce traveling time, seven fjords are suggested crossed by bridges or tunnels, replacing the current ferry crossings. Many of the spans are challenging due to the large spans and deep water depths, and the project is still in an early stage, where the feasibility of different bridge designs are evaluated.

Figure 1.1: Map over E39 and the proposed fjord crossings (taken from *nrk.no*)

Figure 1.2: Illustration of bridge concept (taken from *nrk.no*)

This project will be looking at the bridge design proposed in the report *Curved Bridge - Navigational Channel in South*, developed in cooperation between COWI, Aas Jakobsen, Johs Holte As and Global Maritime. The bridge is a 4603 meter long curved floating bridge going from Svarvhelleholmen in the south to the sea bottom summit Flua in the north. A separate bridge concept will be used for the remaining span from Flua to land, and this is not part of the design analyzed in this project.

The bridge is floating freely without moorings and has a curved shape to help carry shear forces by membrane action. The navigation channel is located in the south end, where the bridge is elevated to allow ships to pass under the bridge girder. This section is cable-stayed with a cable tower grounded on rocks at Svarvhelleholmen, an islet close to shore at the south side of the fjord.

The ship traffic in the area poses a risk for collisions with the bridge, in particular for the pontoons closest to the navigational channel. The strength of the bridge against such accidental events thus needs to be assessed. In this project dynamical ship impact analyses are conducted in the software USFOS, to investigate the global strength of the bridge against such accidental loadings.

To set a basis for the collision analysis a theoretical background for the analysis is presented. For the type of analyses run in this thesis, most of the effort goes into developing the model used. A brief presentation is included for this work, although most details had to be excluded. This is partly to keep the report concise and to the point, but also to protect the work. Both from plagiarism of the work done in the thesis, but also because details about the bridge design could be a significant competitive advantage for COWI and the other contributing companies. Some introductory analysis on the damping, ballasting of the bridge, as well as an eigenvalue analysis, were also performed, to set a base for the main collision analyses.

Because the project is still in the early stages, there are many uncertainties associated with the design, and the loads the to which the bridge will be exposed. The goal of the analyses would thus not be to determine the response and the stresses in the bridge exactly since details in the background for the analysis might change as the project moves on. Observing the overall trend of the response, and determining what parts of the bridge will need strengthening would instead be the focus.

Chapter 2

Theory

2.1 Solution in Time Domain

When solving a dynamical problem in the time domain, the relationship between the response and the physical properties are simplified into the dynamical equation of motion, shown in equation 2.1. Finding the response of the structure thus means solving for the nodal acceleration, $\ddot{\mathbf{q}}$, velocity, $\dot{\mathbf{q}}$, and displacement, $\mathbf{q}$. Doing so in the time, domain means that the response is found, one time-increment at the time. Usually, $\ddot{\mathbf{q}}$, $\dot{\mathbf{q}}$, and $\mathbf{q}$ must be known for the initial time step, whereas the response for the next timestep is found based on this information. By incrementally solving for the response at the next time step t_{n+1}, by using the information from t_n, the whole response history would be developed gradually.

$$\mathbf{M}\ddot{\mathbf{q}} + \mathbf{C}\dot{\mathbf{q}} + \mathbf{K}\mathbf{q} = \mathbf{Q}(t) \tag{2.1}$$

2.1.1 HHT-α Method

Several different algorithms can be used to give the relationship between the incremental time steps to solve the dynamical equation of motion. In the USFOS software, the Hilbert-Hughes-Taylor-α method (HHT-α) is used (Marintek, 2001), which is a more general form of the Newmark-β method. In this section, a brief overview of these methods are presented, based on the information given in Negrut, Ottarsson, Rampalli and Sajdak (2005)

The Newmark method defines the integration formulas given in Equation 2.2 and 2.3 (Negrut, Ottarsson, Rampalli and Sajdak, 2005). By the use of these formulas, $\dot{\mathbf{q}}_{\mathbf{n+1}}$ and $\mathbf{q}_{\mathbf{n+1}}$ are expressed through the accelerations $\ddot{\mathbf{q}}_{\mathbf{n+1}}$, as the only unknown (when the response at time step n is already known).

$$\mathbf{q}_{n+1} = \mathbf{q}_n + h\dot{\mathbf{q}}_n + \frac{h^2}{2}[(1-2\beta)\ddot{\mathbf{q}}_n + 2\beta\ddot{\mathbf{q}}_{n+1}] \tag{2.2}$$

$$\dot{\mathbf{q}}_{n+1} = \dot{\mathbf{q}}_n + h[(1-\gamma)\ddot{\mathbf{q}}_n + \gamma\ddot{\mathbf{q}}_{n+1}] \tag{2.3}$$

This can then be used to give a discretization of the equation of motion, at the next time-step, t_{n+1}, as shown in Equation 2.4 (Negrut, 2005).

$$\mathbf{M}\ddot{\mathbf{q}}_{\mathbf{n+1}} + \mathbf{C}\dot{\mathbf{q}}_{\mathbf{n+1}} + \mathbf{K}\mathbf{q}_{n+1} = \mathbf{F}_{n+1} \tag{2.4}$$

The acceleration is the only unknown and can be found by solving the linear system. This method is second order accurate, and unconditionally stable, as long as equation 2.5 is fulfilled. The main setback with this method, is that it does not inhere a desirable level of numerical damping. This makes the method impractical for problems where high-frequency oscillations are not of interest, or in the case of parasitic oscillations.

$$\gamma \geq \frac{1}{2} \quad , \quad \beta \geq \frac{(\gamma + \frac{1}{2})^2}{4} \tag{2.5}$$

The HHT-α method improves upon this method by introducing a third parameter α that introduce numerical damping. The damping introduced is largest for the higher order vibration modes, which means that it will eliminate parasitic terms of a higher order, and remove noise from the solution. The numerical damping increase as the value of α decrease, but for an α equal to zero, the method will condense to the Newmark-β method, with no damping. The discretization of the dynamical equation given by the HHT-α method, is provided in Equation 2.6.

$$\mathbf{M}\ddot{\mathbf{q}}_{\mathbf{n+1}} + (1+\alpha)(\mathbf{C}\dot{\mathbf{q}}_{\mathbf{n+1}} + \mathbf{K}\mathbf{q}_{n+1}) - \alpha(\mathbf{C}\dot{\mathbf{q}}_{\mathbf{n}} + \mathbf{K}\mathbf{q}_{n}) = \mathbf{F}(\tilde{t}_{n+1}) \tag{2.6}$$

Where $\tilde{t}_{n+1}$ is given by Equation 2.7

$$\tilde{t}_{n+1} = t_n + (1+\alpha)h \tag{2.7}$$

The method will be unconditionally stable given that 2.8 is fulfilled

$$\alpha \in [-\frac{1}{3}, 0] \quad , \quad \gamma = \frac{1-2\alpha}{2} \quad , \quad \beta = \frac{(1-\alpha)^2}{4} \tag{2.8}$$

Chapter 3

USFOS Model

3.1 Introduction

For the analyses in this Master's Thesis, the software USFOS is used. The model is based on the bridge design given in the report *Curved Bridge – Navigational Channel in South (2016)* by COWI, Aas-Jakobsen, Johs Holt AS and Global Maritime.

An initial suggestion for the USFOS model was developed by post. doc. Yanyan Sha and used as the starting point for the analyses. After obtaining the model, all the geometries were controlled and compared to the geometry given in COWI (2016) and bridge drawings(COWI, Aas-Jakobsen and Johs Holt AS (2015)) for the same design obtained through Supervisor Prof. Jørgen Amdahl.

The whole model is controlled and reassessed to have control over all the aspects of the modelling that could affect the accuracy of the results. This task introduced the major part of the work for this Masters Thesis, and showed to be very time consuming. A large number of alterations were done to improve the model, and some of these are described briefly in the end of this chapter. A detailed description of all the work done on the model are however not included in this Thesis. This is because the number of calculations done are too high, and including them in the thesis would make it unnecessary lengthy. To keep it concise, only a brief presentation of models parameters are thus presented, together with the most important alterations and flaws.

As discussed in the preface, it is decided to censor some of the details for the model to protect the structural details of the design developed by COWI et al. This was done by hiding the numbers with black markings, for a number of the tables and figures in this chapter. This should however not be too important for understanding how the bridge is modelled since the overall geometry and the work done in the thesis is not censored.

3.2 Geometries

3.2.1 Cable Wires

The wires for the cable stayed section are modeled with thick walled pipes, and defined as riser elements, which will protect them from buckling, should they experience compressive forces. The cross sectional area for each individual wire was presented in COWI et al.(2016), changing from a minimum of 6900 [mm^2] to 13800 [mm^2]. To avoid creating a unique cross section for each wire, the cross sectional areas were divided into intervals of 250 [mm^2] and each wire were assigned a cross section corresponding to one of these intervals. The intervals, and the corresponding cross sections are given in Table 3.1.

Table 3.1: Wire cross section

Cross section	Interval [mm^2]	Diameter [mm]	Wall thickness [mm]
101	6750 - 7000	150	16.4
102	7000 - 7250	150	17.1
103	7250 - 7500	150	17.8
104	7500 - 7750	150	18.4
105	7750 - 8000	150	19.2
106	8000 - 8250	150	19.9
107	8250 - 8500	150	20.6
108	8500 - 8750	150	21.3
109	8750 - 9000	150	22.1
110	9000 - 9250	150	22.8
111	9250 - 9500	150	23.6
112	9500 - 9750	150	24.4
113	9750 - 10000	150	25.2
114	10 000 - 10 250	150	26.0
115	10 250 - 10 500	150	26.8
116	10 500 - 10 750	150	27.6
117	10 750 - 11 000	150	28.5
118	11 000 - 11 250	150	29.3
119	11 250 - 11 500	150	30.2
120	11 500 - 11 750	150	31.1
121	11 750 - 12 000	150	32.0
122	12 000 - 12 250	150	33.0
123	12 250 - 12 500	150	33.9
124	12 500 - 12 750	150	34.9
125	12 750 - 13 000	150	35.9
126	13 000 - 13 250	150	36.9
127	13 250 - 13 500	150	38.0
128	13 500 - 13 750	150	39.1
129	13 750 - 14 000	150	40.2

3.2.2 Pontoons

The geometry of the pontoons are shown in Figure 3.1. In USFOS, buoyancy elements are used to model the pontoons, which means the pontoons could not be represented with the curved edges, but will instead be modeled as rectangular barges, where the flanges are excluded. The geometry used in the model is shown in Figure 3.2, and it is seen that the model thus gives a too high displacement.

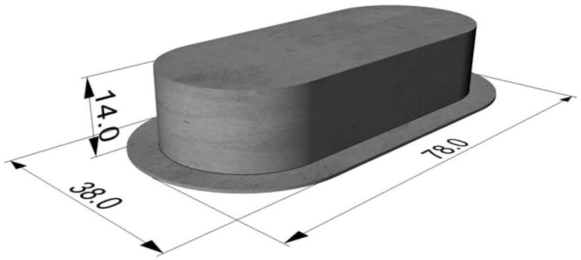

Figure 3.1: Pontoon geometry (COWI et al. (2016))

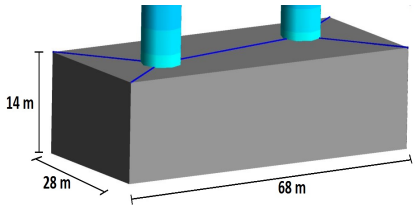

Figure 3.2: Modeling of pontoon

The directions of the pontoons which will be referred to throughout this Thesis, is defined in Figure 3.3. This is definition is not coherent with the definition used in COWI et al. (2016).

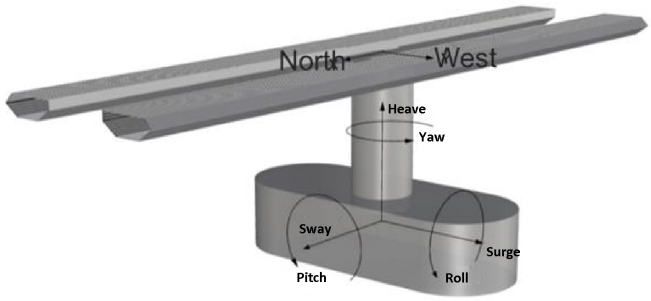

Figure 3.3: Definition of directions used when refering to the pontoon motion. Picture taken from COWI et al. (2016), but definition of the surge, sway, roll and pitch motions are opposite from in that report.

3.2.3 Springs for Water-plane Stiffness

The buoyancy elements discussed in the previous section, only introduce water-plane-stiffness in heave motion. Therefore the stiffness in pitch and roll have to be introduced through springs. This is done by specifying a stiffness against displacements in respective degrees of freedom, at specific nodes. By introducing the springs at a node in the centre of the pontoon, the rotational stiffness of the pontoon, can be introduced directly with the values found in COWI et al. (2016).

The lack of rotational stiffness for the buoyancy elements caused a lot of trouble during the modeling, since this flaw was not known in advance, and no documentation were available for the buoyancy element type. After reoccurring crashed of the analysis, investigations on

one single pontoon were thus conducted. A description of this investigation can be found in Appendix 10.1.

In the eigenvalue analysis, the heave stiffness from the buoyancy calculation have no effect, since the hydrodynamical calculations are excluded. The heave stiffness will thus also be represented by a spring, when running the eigenvalue analyses. The exact stiffness for the springs used in the pontoons are given in Table 3.2

Table 3.2: Waterplane stiffness of pontoons(directions defined as in COWI et al(2016))

Motion	Waterplane stiffness
Roll	5.7E+9 Nm/rad
Pitch	1.0E+9 Nm/rad
Heave	1.75E+7 N/m

3.2.4 Bridge Girder

The bridge girder consists of two beams, one for each of the pathways, connected by transverse beams. The pathways have symmetric cross sections, and the geometries for the left pathway are given in Figure 3.4 and 3.5. There are two different geometries for these cross sections, one for the main part of the bridge, and a smaller one for the high part of the bridge supported by cable wires.

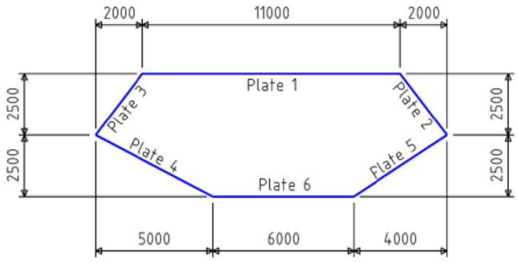

Figure 3.4: Cross section for cable stayed part of bridge. (COWI et al. (2016))

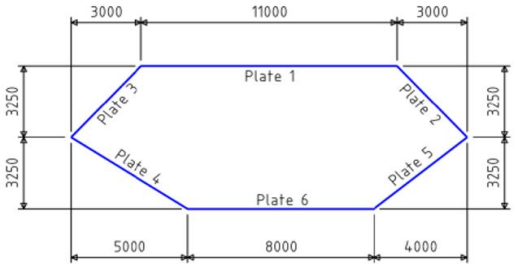

Figure 3.5: Cross section for main part of bridge. (COWI et al. (2016))

The thickness of the plating in the cross section is also varied over different parts of the bridge to increase the strength of the cross section in certain areas. The data for the different cross sections are given in Table 3.3 and 3.4, and their locations on the bridge are shown in Figure 3.6. The small geometry is used for cross-section H1,H2 and H3, while the large geometry is used for cross-section F1, F2, S1, S2*, S2, S3* and S3.

Table 3.3: Cross sectional properties (Details censored)

Cross section name	H1	H2	H3
Equivalent plate thickness [mm]			
Plate 1	[redacted]		
Plate 2	[redacted]		
Plate 3	[redacted]		
Plate 4	[redacted]		
Plate 5	[redacted]		
Plate 6	[redacted]		
Cross sectional area [m^2]	[redacted]		
Iz(strong axis)[m^4]	[redacted]		
Ix(weak axis)[m^4]	[redacted]		
It(torsion)	[redacted]		
Wpx [m^3]	[redacted]		
Wpz [m^3]	[redacted]		
Wpt(torsion)	[redacted]		

Table 3.4: Cross sectional properties (Details censored)

Cross section name	F1	F2	S1	S2*	S3*	S3
Equivalent plate thickness [mm]						
Plate 1	[redacted]					
Plate 2	[redacted]					
Plate 3	[redacted]					
Plate 4	[redacted]					
Plate 5	[redacted]					
Plate 6	[redacted]					
Cross sectional area [m^2]	[redacted]					
Iz(strong axis)[m^4]	[redacted]					
Ix(weak axis)[m^4]	[redacted]					
It(torsion)	[redacted]					
Wpx [m^3]	[redacted]					
Wpz [m^3]	[redacted]					
Wpt(torsion)	[redacted]					

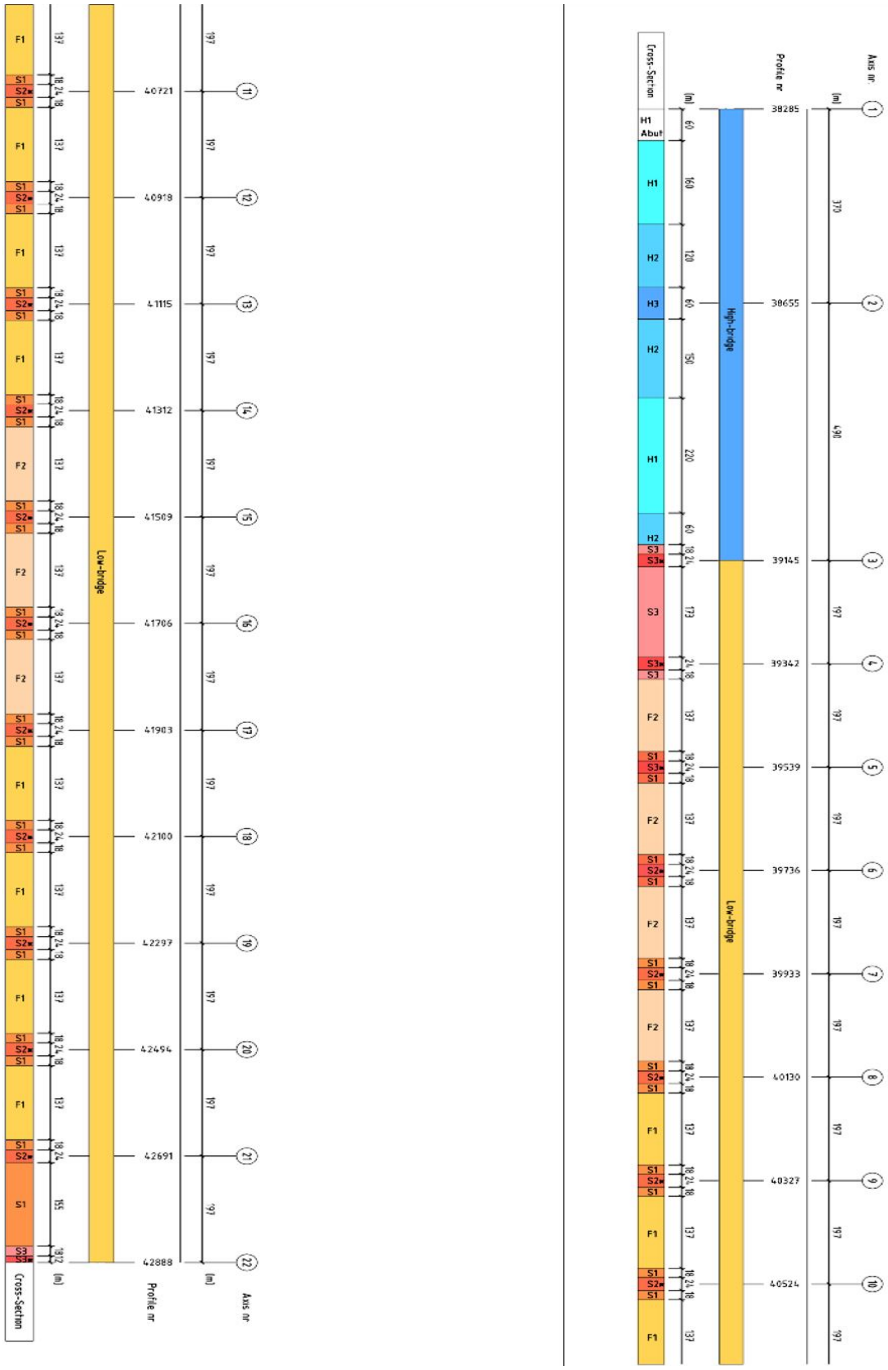

Figure 3.6: Location of different cross sections on the bridge girder (COWI et al. (2016))

3.2.5 Added Mass

Added mass are introduced to the pontoons in the analysis with the values given in Table 3.5. This is done by giving the added mass property to the rigid beam between the columns, as seen in Figure 3.2. The rotational added mass of the pontoons could not easily be introduced, and are thus neglected in the model.

The value of the added mass are found in the COWI et al. (2016) as a function of the oscillation period. The added mass used in the analyses are the value found for periods above 20 seconds, because it is expected that these modes will be the governing motions in the ship impact analysis. This will not be correct for the smaller eigenmodes in the eigenvalue analysis, but since the added mass can not vary during the analysis, and the larger modes are expected to be more important for ship collision analyses, this choice is made. This choice is discussed further in Section 8.1.2

Table 3.5: Added mass of pontoons(direction defenitions from cowi)

Motion	Added mass [Mkg]
Surge	[redacted]
Sway	[redacted]
Heave	[redacted]

3.2.6 Cross Beams

The two pathways of the bridge girder are connected with cross-going beams every 40 to 50 meters. These help keep the bridge girder act as a whole beam without too much motion between the pathways. The strength of these beams are thus important for the global strength of the bridge and the structural properties are calculated accordingly. Table 3.6 gives information about the geometric properties of the cross-beams, whereof some of the properties are found in the report, and others are calculated based on the geometry.

Table 3.6: Cross beam dimensions. Values marked by "*" are found in the report, while the rest are calculated

	High Bridge	Floating bridge
cross sectional area* [m]	[redacted]	
width of cross section* [m]	[redacted]	
Height of cross section* [m]	[redacted]	
plate thickness top/bot* [m]	[redacted]	
plate thickness walls* [m]	[redacted]	
Iz* [m^4]	[redacted]	
Iy [m^4]	[redacted]	
W_{cz}* [m^3]	[redacted]	
W_{pz} [m^3]	[redacted]	
W_{cy} [m^3]	[redacted]	
W_{py} [m^3]	[redacted]	

3.2.7 Columns

The pontoon columns have 8 meter diameter. All columns from axis 9-21 are 7.5 meter long, while the length increase for axis 8 towards axis 3. Because the length of the columns are increasing the columns from axis 3-6 are strengthened with a effective plate thickness of 60 mm instead of 40mm which is governing for the other columns. See Figure 3.6 for the definition of the axes.

3.2.8 Permanent Loads- asphalt and railings

Because the contribution to the strength of the structure is minimal from components like the railing and asphalt, this is not included in the model. The weights from these are however important to include. Because these loads act directly onto the bridge girders, the weight is included by increasing the steel density of the bridge girders.

Table 3.7: Permanent loads high bridge

Cross section	H1	H2	H3
girder weight load[kN/m]			
Asphalt,railing etc.[kN/m]			
Total permanent loads[kN/m]			
New density[kg/m^3]			

Table 3.8: Permanent loads floating bridge

Cross section	F1	F2	S1	S2*	S3	S3*
girder weight load[kN/m]						
Asphalt,railing etc.[kN/m]						
Total permanent loads[kN/m]						
New density[kg/m^3]						

The report gives the loads from the asphalt and railings as-well as the load of the self-weight of the girder as can be seen in Table 3.7 and 3.8. By deviding the total permanent loads by the load from the girders self weight, the factor of which the density should be increased with is found. This is done for all the different bridge cross sections, and the resulting density can be found in Table 3.7 and 3.8.

3.3 Improvements of Original Model

The model obtained from post doc Yanyan Sha, were an initial suggestion, where the cross sectional and material properties were not very accurate. A throughout control of the model was thus conducted, where all properties were calculated correctly. Due to the large numbers of calculations, these will not be included in this report, but in this section, a selection of the most important improvements are presented.

3.3.1 Lowering of the Bridge Girder

Due to the lack of specification in the bridge drawings, the height of the bridge girder was wrong in the bridge obtained from Yanyan Sha. The position of the bridge girder given in the drawings gave the top of the bridge girder instead of the centerline, which was first assumed. To improve this, the whole girder had to be lowered, by changing the z coordinates of all the nodes for the girder and cross beams.

On top of that the, inclination in the rising part of the bridge was not accurately modeled. The inclination of 3.9 percent which was given for parts of the rising bridge, was used for the whole rising part, which was not correct. In the updated model the inclination was calculated by finding the constant inclination needed for a constant slope between axis 3 and 8, as well as a constant slope between axis 2 and 3. This change resulted in the z-coordinate of the bridge girders center-line to change from 56.33 meter, to 49.27 meter at axis 3. The height was thus off by more than 7 meters originally, which could have caused a significant error in the results.

3.3.2 Girder Cross-sectional Properties

In the original model, the cross sectional properties of the bridge was not modeled correctly. One, single cross section was used for the whole bridge length, but as seen in Section 3.2.4 the cross section should differ to give extra strength to certain parts of the bridge. This had to be improved before moving on with the analyses.

3.3.3 Cable Wires

To improve the model, the strength of the wires were modeled more accurately. In the original model all the wires had the same cross section, and the strength were higher than what was suggested in the COWI et al. (2016), based on their ULS check. To get a more realistic model, the cables was thus modeled as described in Section 3.2.1.

3.3.4 Springs for Water-plane Stiffness

In the original model, the springs used for the water-plane stiffness were connected in the two node points at the bottom of the pontoon columns. The problem with doing so, is that due to the distance from the rotational centre of the pontoon to the applied springs, the springs with stiffness in the vertical direction, would also contribute to rotational stiffness for the pontoon.

By moving the springs to the centre of the pontoon, this problem was avoided, and the water-plane stiffness could be modeled more exact.

3.4 Pre-tension and Error in Initial Stresses

The wires for the cable-stayed bridge are intended to be pre-tensioned, to support the weight of the bridge girder. In USFOS, such a pre-tension is not possible to model properly. When applying weight to the structure, the bridge will thus deform until the elongation of the wires are large enough for the forces in the wires to balance the weight. This will result in an equilibrium condition where the bridge girder at the centre of the main span, deflect several meters, giving a geometry differing from what should be modeled.

To correct for this geometry error, the command HJHansen are used. The stresses in the bridge at equilibrium are found, before the geometry are reset to the initial geometry, while the stresses found are kept. As can be seen from Figure 3.7, this introduce large stresses in the bridge girder, that are caused by bending of the bridge girder. In reality this bending stress would not be present, because the pretension in the wires would prevent the deflection of the bridge girder. The lack of pretension in the model thus causes the bridge to support a lot of the weight by bending. Weight that in reality would have been supported by tension in the cables. The result is a model that give too high stresses in the bridge girder, while the stresses in the cables are lower than in reality.

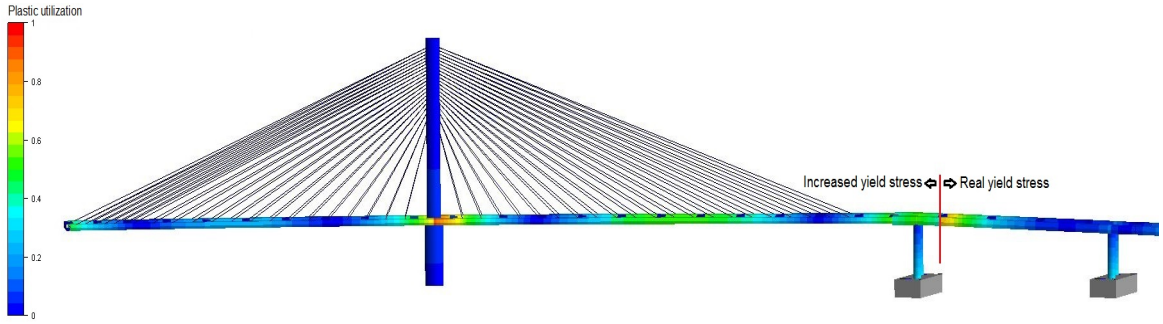

Figure 3.7: Plastic utilisation from permanent loads. Yield stress set to two times the correct value for the bridge girder left of the position marked with the red line

Due to this flaw in the modeling software, the stresses in some areas of the cable stayed section are close to the yield stress when the permanent loads are applied. To be able to run the analyses without large plastic deformations initially, the yield stress are thus increased by a factor of 2, for the bridge girder left of the position marked with a red line in Figure 3.7.

When running the ship collision analyses, the plastic utilization factor is used as the measure of the remaining global strength of the bridge. This factor is a measure of the loading in the bridge members, in relation to the loading that would cause plastic deformations. It is thus directly related to the yield stress of the material. For the parts of the bridge where the yield stress is doubled, a plastic utilization factor of 0.5 would thus give plastic deformations.

Since the utilization factor due to the initial permanent loads are already above 0.5 in some parts of the bridge, using this as a limit would not be possible. Instead the increase in the utilization factor, due to the ship collision, would be investigated for these parts of the bridge. The increase in the utilization factor will be independent of the initial utilization, as long as the material

stays in the elastic domain. The results would thus be correct, even if the initial utilisation factor is wrong. How large of an utilization increase that could be accepted, would of course be dependent on what the utilization from the permanent loads are in reality. Before drawing a clear conclusion on whether the global strength of the bridge would be able to withstand the ship collisions, these initial stresses must be thus found. This could not be done using the USFOS software due to the lack of options for representing the pre-tension in the wires, and a separate analysis must therefore be developed. However, by presenting the results as the increase in plastic utilization, the results of this analysis could be combined with the determined initial stresses, to give a final conclusions on whether the bridge would survive the collision scenarios investigated.

For the most parts of the bridge, the initial stresses are estimated fairly correctly, and as seen in Figure 3.7 the correct yield stress are used for these parts. For the bridge girder of the cable-stayed section, however the increase in the plastic utilization factor have to investigated. For the rest of the bridge, one could simply look at the value of the plastic utilization factor to determine if plastic deformations would occur.

Chapter 4

Weight Equilibrium

In the drawings available for the bridge, no information is given about the ballasting of the pontoons. As a first approximation, rough calculations for the weight of the bridge is conducted using the volume of steel multiplied by the steel density. The permanent loads of the asphalt and railings from Section 3.2.8 are also included in these calculations. The buoyancy of each pontoon is easily found by the submerged volume of the buoyancy element. By assuming that there should be equilibrium between the buoyancy of the pontoon, and the weight each of the pontoons support, the weight of the ballast can be found. Because there are no fast way of estimating for example how much of the cable stayed section that is supported by the pontoon, and how much is supported by the column at axis 2, these calculations would only yield a rough estimation.

When first running the dynamical analysis, it can be seen that the ballasting was not correctly distributed, and the submergence of the pontoons are incorrect. In Figure 4.1 the initial distribution of the ballast is shown with the displacements scaled by a factor of ten. It is evident that for example for the pontoons at axis 3 and 4, the weight should be reduced. By trial and error, the correct ballasting is found. Figure 4.2 show the final result, where the free-board for all the pontoons vary with less than 4 cm for all the pontoons, which is accepted as a very accurate estimation for the ballasting.

Figure 4.1: Illustration of incorrect distribution of ballasting. Displacements scaled by 10

Figure 4.2: Final distribution of ballasting. Displacements scaled by 10

Chapter 5

Eigenvalue Analysis

5.1 Theory

The natural frequencies, or the eigenfrequencies of a structure, are the frequencies the structure tends to vibrate in when it is oscillating freely. For an intricate structure like the bridge examined in this thesis, large number of such frequencies exist. One corresponding to each of the natural response modes or eigenmodes, that the structure would vibrate in.

When vibrating freely without damping or other forces acting on the structure, the equation of motion could be written as in Equation 5.1.

$$\mathbf{M\ddot{r}} + \mathbf{Kr} = 0 \tag{5.1}$$

In order to solve this equation, an harmonic function 5.2 are introduced (Langen and Sigbjørnsson, 2007, page 4.1).

$$\mathbf{r} = \phi sin(wt) \tag{5.2}$$

Where ϕ is the mode-shape or eigenvector, and ω is the angular frequency. By inserting this function into the equation of motion, the eigenvalue equation as seen in equation 5.3 are obtained.

$$(\mathbf{K} - \omega^2\mathbf{M})\phi = 0 \tag{5.3}$$

By solving this equation the different eigenmodes, ϕ, and eigenfrequencies ω, can be found.

Running an eigenvalue analysis is often a first step when running a dynamical analysis. This is because the results from the eigenvalue analysis give a good understanding of the structural behaviour of the structure, as well as provide an indication of how the structure will respond to different loading. (Siemens, 2014, page 4.2)

5.2 Work

As seen in the previous section, the eigenvalue analysis is based on the mass and stiffness matrices of the structure. It is thus important that these are represented correctly in the model.

The pontoons of the bridge are modeled with buoyancy elements, and as described in Section 3.2.3 the water plane stiffness in heave is calculated through hydrodynamical calculations on the pontoons. In the eigenvalue analysis these hydrodynamical calculations are not included, and the stiffness in heave must thus be introduced through springs, as was done for the roll and pitch moments.

The added mass are also added manually, as properties for the beam element connecting the columns of the pontoon, instead of being calculated by automatically by the software from the buoyancy elements.

5.3 Results

After making the changes to the bridge, and finishing the pontoon ballasting, an eigenvalue analysis is conducted. This gives insight on how the bridge will behave under certain loads. Looking at the different mode-shapes can help determine in which position on the bridge, a collision will give the larges motions. (hopefully this is done later in the thesis, and a reference to that section can be made here)

The eigenvalues found in the analysis are presented in Table 5.1, together with a simplified description of each of the eigenmodes. The eigenmodes are illustrated in Figure 5.1 to 5.6, by showing the displacements scaled by a factor of 30, on top of the initial geometry. The next 14 eigenmodes are given in the appendix in section 10.2.1.

Table 5.1: List of the 20 largest eigenvalues of the bridge. Including a description of the type of motion.

Mode number	Eigenvalue	type of motion
1	62.66	horizontal bending
2	36.44	horizontal bending
3	20.76	horizontal bending with twisting
4	19.85	horizontal bending with twisting
5	14.28	horizontal bending with twisting
6	11.93	vertical bending
7	11.87	vertical bending
8	11.80	vertical bending
9	11.71	vertical bending
10	11.59	vertical bending
11	11.44	vertical bending
12	11.21	vertical bending
13	11.02	horizontal bending with twisting
14	10.87	vertical bending with twisting
15	10.43	vertical bending
16	10.25	twisting
17	9.92	vertical bending with twisting
18	9.54	twisting
19	9.36	vertical bending with twisting
20	8.78	vertical bending with twisting

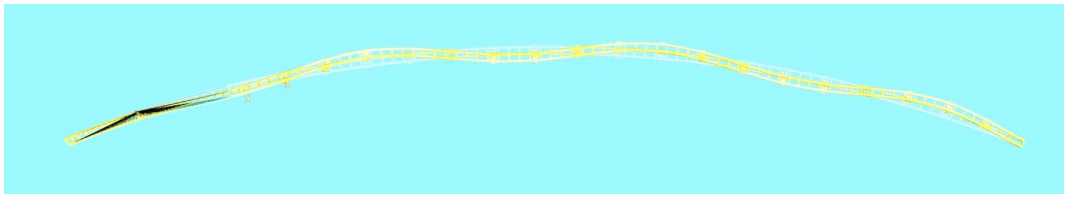

Figure 5.1: Eigenmode with eigenperiod of 62.66 seconds

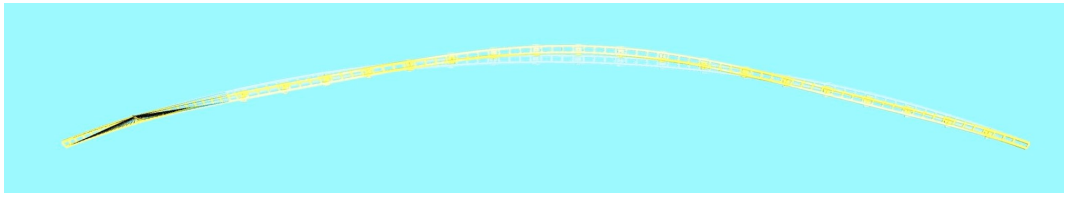

Figure 5.2: Eigenmode with eigenperiod of 36.44 seconds

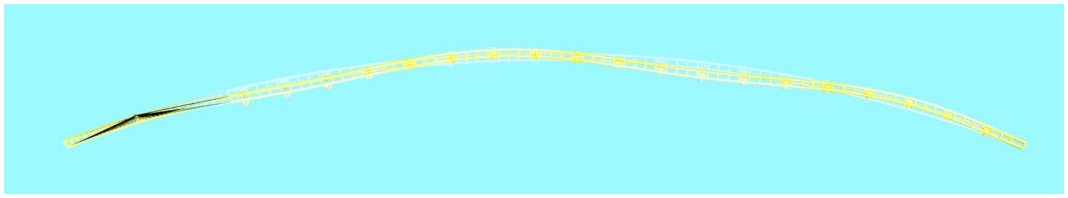

Figure 5.3: Eigenmode with eigenperiod of 20.76 seconds

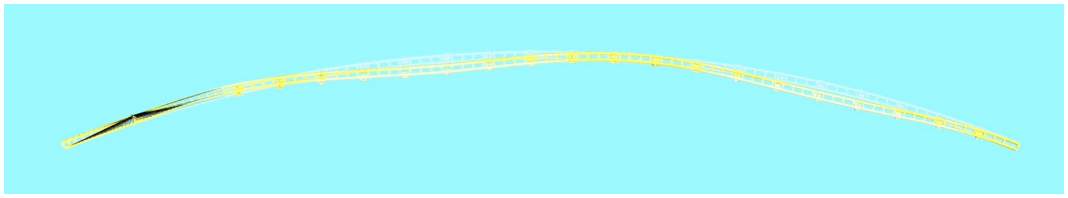

Figure 5.4: Eigenmode with eigenperiod of 19.85 seconds

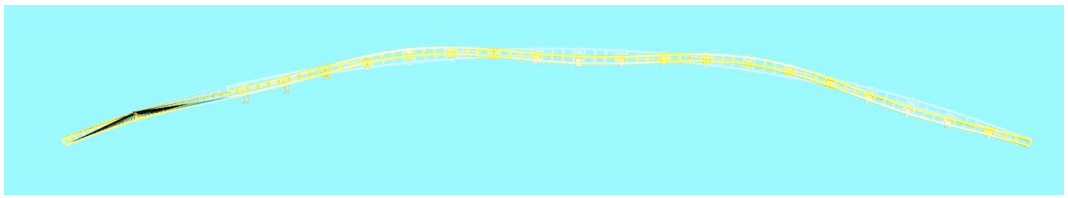

Figure 5.5: Eigenmode with eigenperiod of 14.28 seconds

Figure 5.6: Eigenmode with eigenperiod of 11.93 seconds

Chapter 6

Damping

There are significant uncertainties connected to the representation of the damping in the model used for the analyses. This can have a large effect on the results, and it is therefore important that the damping level used is clearly presented. At a later stage, a better estimation of the damping level might be developed. It is thus interesting to see the effect of changing the damping parameters, to see how an error in the damping representation affects the results of the analysis. One could thus get an impression of how the results of the analysis would look like with damping parameters differing from those used in main analysis, without having to rerun the analyses. The damping level for the prima analyses have been set at a level that are expected to be somewhat lower than the real value, so that the damping do not damp out important aspects of the response.

A theoretical background for the damping used in the analysis are presented in this chapter, together with a presentation of the damping levels used. A description of, as well as the results from the damping sensitivity study will also be presented.

6.1 Theory

In structures like the floating bridge analysed in this thesis, there are several sources to damping forces. It is normal to distinguish between two main types of damping, the structural and the hydrodynamical damping. The structural damping is the damping related to the internal friction in the material of the structure, while the hydrodynamical damping is due to the waters interaction with the submerged pontoons.

6.1.1 Structural Damping

In the analysis, proportional damping, also called Rayleigh damping is used to represent the structural damping. A short presentation of this damping theory, based on information from Langen and Sigbjørnsson (2007, page 9.25), is thus presented in the following section.

Rayleigh damping assumes that the damping is proportional to a coupling between the velocity, and the strain velocity at each node-point, giving the relation between the damping and the mass and stiffness matrices, $\mathbf{M}$ and $\mathbf{K}$, as shown in Equation 6.1.

$$\mathbf{C} = \alpha_1 \mathbf{M} + \alpha_2 \mathbf{K} \tag{6.1}$$

The damping ratio λ, which gives the ratio between the damping and the critical damping, are for Rayleigh-damping given by Equation 6.2

$$\lambda_i = \frac{\bar{c_i}}{2\bar{m}_i\bar{\omega}_i} = \frac{1}{2}(\frac{a_1}{\omega_i} + a_2\omega_i) \tag{6.2}$$

From this it is seen that the damping ratio for all frequencies can be found, if the values for α_1 and α_2 are known. By specifying the damping ratios λ_1 and λ_2 for two different frequencies ω_1 and ω_2, the value for α_1 and α_2 can be found from equation 6.3. In this way the damping ratio for the whole frequency range can be found, and customized by controlling λ_1 and λ_2 and their corresponding frequencies.

$$\alpha_1 = \frac{2\omega_1\omega_2}{\omega_2^2 - \omega_1^2}(\lambda_1\omega_2 - \lambda_2\omega_1) \qquad \alpha_2 = \frac{2(\omega_2\lambda_2 - \omega_1\lambda_1)}{\omega_2^2 - \omega_1^2} \tag{6.3}$$

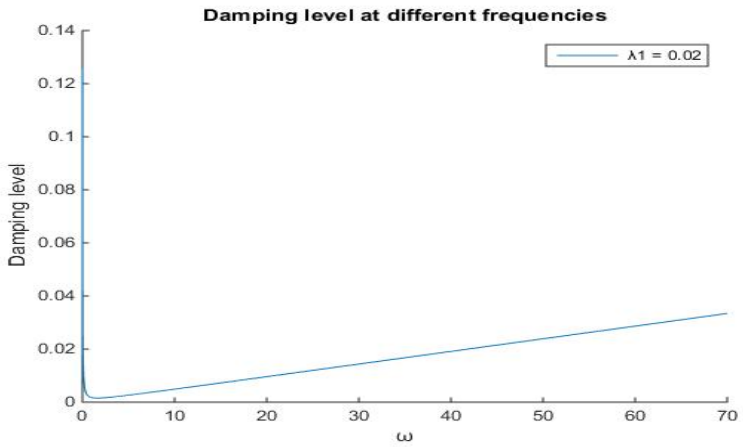

Figure 6.1: Rayleigh damping

6.1.2 Hydrodynamical Damping

In additional to the structural damping added through Rayleigh damping, there are hydrodynamical damping on the pontoons. Hydrodynamical damping is assumed to be composed of two parts (Langen and Sigbjørnsson (2007, page 9.13)):

- geometrical damping
- drag damping

The geometrical damping is also called radiation or diffraction damping and is caused by structural vibrations that generate waves in the fluid around the structure. The drag damping is due to viscous effects and vortex shedding in the water around the structure.

The drag forces on a submerged body is given by the drag equation, 6.4, where the velocity u, is set as the relative velocity between the pontoons and the water particles. The drag force will thus always work against the motion in still water, and give damping of the excitations.

$$F_{drag} = \frac{1}{2}\rho u^2 C_{drag} A \tag{6.4}$$

Where ρ is the water density, u is the relative velocity between the water and the body, A is the cross sectional area, and C_{drag} is the dimensionless drag coefficient.

The geometrical damping from diffraction can be found by Equation 6.5, an this is the definition used by the software Usfos (Information obtained from supervisor Jørgen Amdahl)

$$F_{diff} = \nabla\sqrt{\frac{2g}{D}} u C_{diff} \tag{6.5}$$

where ∇ is the displacement, D is the draught, u is the velocity, g is the gravitational constant and C_{diff} is the dimensionless damping coefficient.

6.2 Work

No information about the damping of the structure are available through the drawings and reports obtained, and appropriate damping levels must thus be developed. The assumptions made in regards to the damping, and the damping sensitivity study conducted, are presented below.

6.2.1 Structural Damping

In guidance with professor Amdahl, it is decided that the structural damping level of 0.5-3 percent, could be a good estimation for such a structure.

With Rayleigh damping, the damping level change for the different oscillation frequencies, and one could thus not get this level of damping throughout the whole frequency spectrum. It is therefore prioritized to get as good of a representation as possible for the frequencies that are most important for the global reaction of the bridge due to the ship collision.

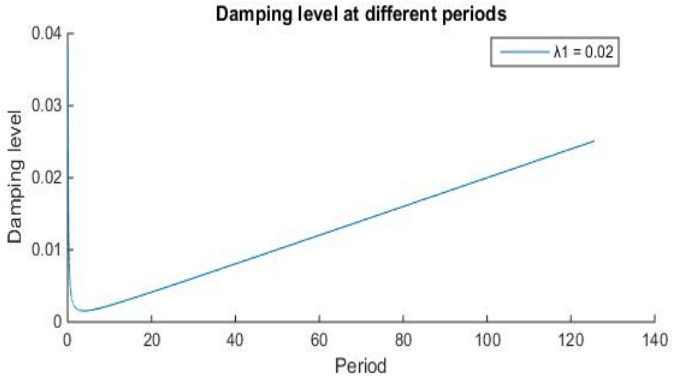

Figure 6.2: Rayleigh damping used in main analyses, plotted for different oscillation periods

In Figure 6.1 the damping level chosen are presented, but with the period along the x-axis, instead of the angular frequency, to make it easier to comprehend. From the eigenvalue analysis it is found that the largest eigenperiod is 62.66 seconds. It is expected that the ship collisions would induce some of the larger eigenmodes, and that these would contribute to large parts of the global response. It is thus decided that these ranges of periods should be prioritised when the damping is set. For the damping level chosen, the damping is around 1.2 percent, for the largest eigenperiod of 62.66 second, which corresponds well to the damping level of 0.5-3 which was expected to be a good approximation. For the lower periods, the damping is decreasing, and might be too low. It is decided that this is a better alternative, than for the damping to be overestimated for critical periods. The parameters of the Rayleigh damping used in the main analyses, and plotted in Figure 6.2 are shown in Table 6.1.

Table 6.1: Parameters used for the Rayleigh-damping

ω_1	0.0628	(100 second period)
ω_2	62.832	(0.1 second period)
λ_1	0.02	
λ_2	0.03	
α_1	0.0025	
α_2	9.54E-4	

To see how using the wrong damping levels will affect the results, a damping sensitivity study is performed. The ship collision analysis from case 1, in Section 7.2 was run several times, with different damping levels, and the difference in the analysis result was observed. Details about this analysis can be found in Section 7.2.5, and will not be described here. A collision energy of 1250 MJ was used, which is lager than the expected collision energy predicted in Section 7.2.1. This was to get large motions so that the effect of the damping would be clear. The results compared in these damping investigations, are the maximum horizontal displacement of the bridge girder at the point of impact, as well as the highest increase in plastic utilization, the same results as checked in the main collision analysis in Section 7.3.1

To make the changes in damping level easy to grasp, only the λ_1 value is changed. This will have the largest effect on the small frequencies, and as discussed previously, this is the modes of highest importance for the global response. The damping levels for the different values of λ_1 are given in Figure 6.3, presented with the period along the x-axis.

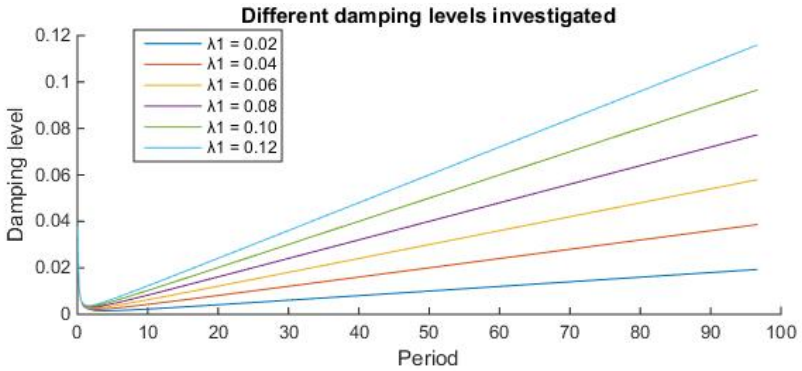

Figure 6.3: Different damping levels investigated in the damping sensitivity study for structural damping

6.2.2 Hydrodynamical Damping

The buoyancy elements in USFOS will automatically calculate the drag and radiation damping, but the drag coefficient and the coefficient for rotational damping must be specified. No information is given for these values, and rough estimations must be made based upon available literature.

In Figure 6.4, the drag coefficient is given for several blunt bodies with varying degree of rounding of the edges. When the edge rounding radius is equal to half of the height, the edge will be a half circle, equal to the rounded edges of the pontoon. For surge motion of the pontoon, a drag coefficient of 0.5 thus seems like a good approximation.

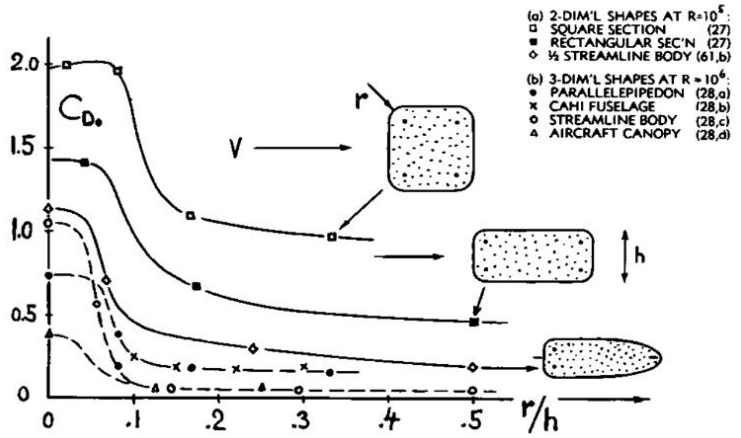

Figure 6.4: Drag coefficients for pressure drag on different blunt bodies, with the effect of rounding radius. (Hoerner, 1965, page 3.13)

In the sway direction, the edges will not be be rounded and the geometry will be somewhere in-between the rectangular and square section. The drag coefficient could thus be somewhere between 1.4 an 2.

For the heave motion of the pontoon, one would assume the drag coefficient to be above 2 due to the effect of the attached flanges at the bottom of the pontoon. No data is available to support this claim however, and the drag coefficient are set to a value of 2, due to lack of a better estimation. In the ship collision analysis, the most important motion will be the surge and sway motion, and this uncertainty is thus accepted. The drag coefficients used in the main analysis are shown in Table 6.2

Table 6.2: Drag coefficients used in main analyses

Motion type	C_D
Surge	0.5
Sway	1.6
Heave	2.0

The values in Figure 6.4 are developed for pressure drag forces, and do not include the friction drag. For such blunt geometries it is natural to assume that the pressure drag forces will dominate, since one would get significant flow separation from the surface body. However,

the concrete of the pontoons might inherent enough roughness for the friction drag to become significant.

The drag force is also for a steady stream, and for a pontoon with oscillatory motions, flow disturbance caused by the pontoon, would affect the drag when oscillating back into its own wake.

No good approximation for the value of the radiation damping was found. Due to the uncertainty around the radiation damping, this damping is set to a very low value, with a damping coefficient of 0.15, which will most probably underestimate the damping, giving a conservative result. The drag damping is probably also a bit underestimated due to the exclusion of friction drag. Overall, the damping of the system would thus most likely be underestimated, which would yield conservative results for the analysis.

As was done for the structural damping, the effect of changing the drag damping was investigated by running collision scenario 1. Different values for the drag coefficients varying from 0.3 to 0.9 was investigated, and the results compared.

6.3 Results

6.3.1 Structural Damping

Figure 6.5 and 6.6, show the effect of the structural damping on the maximum horizontal displacement, and the increase in plastic utilization respectively.

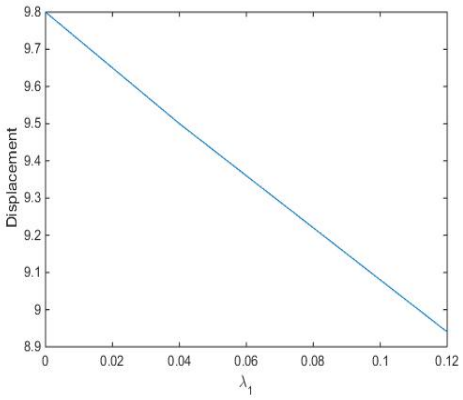

Figure 6.5: Relation between λ_1 of the Rayleigh damping, and the maximum horizontal displacement of the bridge girder at the point of impact

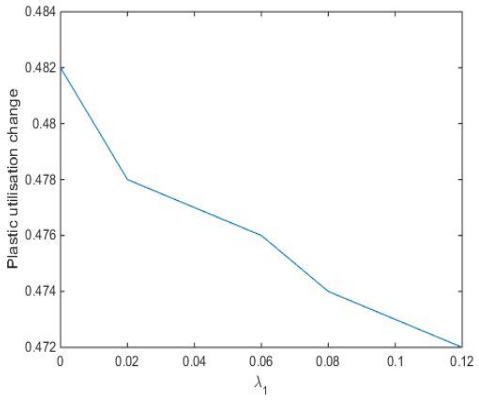

Figure 6.6: Relation between λ_1 of the Rayleigh damping, and the maximum increase in plastic utilisation

It can be seen that as assumed the plastic utilization and the maximum displacement decrease with increasing damping. For the displacement the relation to the damping seems to be almost linear, while for the plastic utilization the effect of changing the damping decrease as the drag coefficient increase. The damping level with λ_1 equal to 0.14, gives 0.86 meter lower displacement compared to the case with zero structural damping. This is a relative decrease of 8.8 percent. For the plastic utilisation, the relative change is 2.1 percent.

6.3.2 Hydrodynamical Damping

Figure 6.7 and 6.8, shows the effect of hydrodynamical damping on the maximum horizontal displacement on the point of impact, as well as the maximum change in plastic utilization.

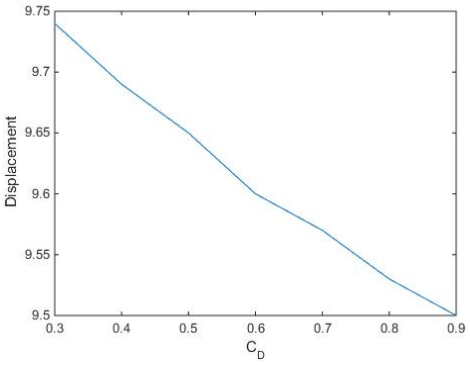

Figure 6.7: Relation between drag coefficient, and the maximum horizontal displacement of the bridge girder at the point of impact

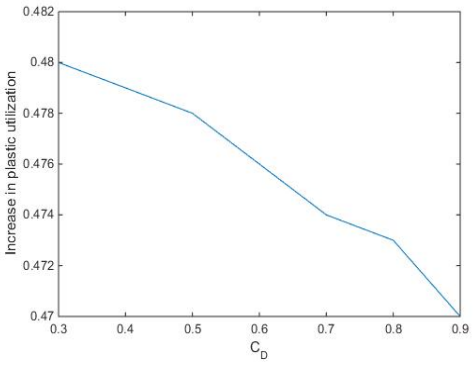

Figure 6.8: Relation between drag coefficient of the Rayleigh damping, and the maximum increase in plastic utilisation

It can be seen that as assumed the plastic utilization and the maximum displacement decrease with increasing damping. For the displacement the relation to the damping seems to be almost linear, while for the plastic utilization the effect of changing the damping increase as the drag coefficient increase. The damping level with a drag coefficient equal to 0.9, gives 0.24 meter lower displacement compared to the case with zero structural damping. This is a relative decrease of 2.5 percent. For the plastic utilisation, the relative change is 2.1 percent.

6.3.3 Concluding Remarks for Damping Investigations

It is seen from the damping investigations that the changes in the final results from the ship collision analysis due to change in the structural and drag damping, is in the order of a few percent for the parameter range investigated. The uncertainties connected to the damping level would introduce significant uncertainties to the final results. The effect on the final results are however small enough for the results to be usable despite some error in the the level of damping.

Chapter 7

Ship Collision

7.1 Theory

7.1.1 Energy Considerations

Annex A in *NORSOK N-004 - Design of steel structures* (2004) deals with design against accidental events, including ship collisions. General theory for ship collisions are presented, and guidelines for doing analyses for this accidental state is given. The following section is based on the information provided in the NORSOK annex when not stated otherwise, and all equations are taken from there(bedre formulering?). Some comments in relation to the particular bridge project are also given.

A ship collision, is highly governed by the kinetic energy involved. Prior to the impact, the mass and added mass of the ship inhere kinetic energy, and during the collision, some of this energy will be dissipated to other parts of the system. A lot of the energy will be transformed into strain energy in the ship and the structure. If the structure is able to move during the collision, some of the energy may also be transferred into kinetic energy by accelerating the structure. For a fixed structure, all kinetic energy must be absorbed as strain, while for a compliant structure some of the energy will remain as kinetic energy.

An installation is assumed to be compliant 'if the duration (of the collision) is small compared to the fundamental period of vibration of the installation'. While 'if the duration of impact is comparatively long, the installation can be assumed fixed'(NORSOK N-004, 2004, Page 88). The eigenvalue analysis executed in this project, will thus be valuable to determine if the bridge can be assumed compliant or not.

A floating bridge as the one analysed in this thesis, have the possibility to be compliant, despite the fixed boundary conditions at both ends. The oscillations in the bridge can take up kinetic energy, causing the structure to be compliant during the collision. Over time the kinetic energy will however be absorbed as strain energy by forming a global bending mode in the bridge, whereas some energy are lost to damping.

The strain dissipation should be investigated at three different levels:

- local cross section
- substructure
- global structure

For the local impact, the plastic strain energy dissipation is the most important, while elastic strain energy will be important for the global bending of the bridge girder. In this thesis, only the global response will be investigated, and the local damage to the structure is not evaluated, as it is not part of task given.

How much of the strain energy that is absorbed by the bridge compared to the ship, will be determined by the strength relation between the two. With relation to this, it is normal to distinguish between three different types of design

- Strength design
- Ductility design
- Sheared-energy design

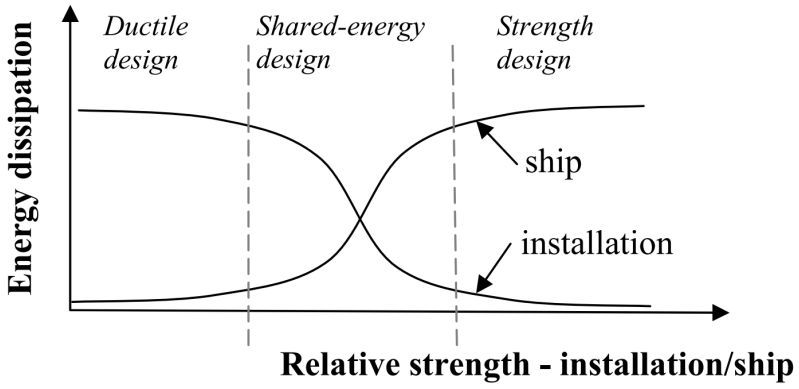

Figure 7.1: Energy dissipation for ductile-, shared-energy- and strength design (*NORSOK N-004 - Design of steel structures* (2004))

With a strength design, the bridge, undergoes little deformation, and most of the strain energy is due to deformation of the ship. For ductility design, the opposite is the case. The bridge is weak compared to the ship, and the strain energy will be mostly due to deformation of the bridge. In shared-energy design, both structures undergo substantial deformations during the collision, and both contributes to the strain energy.

The most realistic model for many ship collisions is the shared-energy model, but this will also be the most demanding model considering calculation costs. For ductility and strength design, the response of the weak structure, can be assumed to follow the shape of the strong structure, which highly simplifies the problem. In shared-energy design however, the deformation shape is also unknown, and the complexity of the calculations are high.

The response of the ship and the installation can be shown using a load-deformation curve as shown in Figure 7.2. Here the deformation of both the ship and the installation is given for corresponding contact loads. The dissipated strain energy for the ship and installation is given by the area under their corresponding load-deformation curve. The total strain energy is the sum of the strain energy for the ship and the installation, as shown in Equation 7.1.

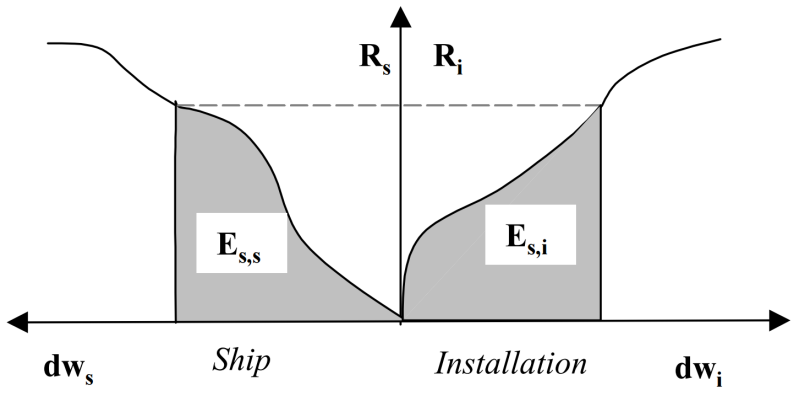

Figure 7.2: Load-deformation curve for a ship and an installation during a collision with shared-energy design (*NORSOK N-004 - Design of steel structures* (2004))

$$E_s = E_{s,s} + E_{s,i} = \int_0^{w_{s,max}} R_s \, \mathrm{d}w_s. + \int_0^{w_{i,max}} R_i \, \mathrm{d}w_i \tag{7.1}$$

7.1.2 Global Modeling

When analyzing the global response of a structure, the structure as a whole would need to be included in the model. In order to keep the number of elements, and the calculation costs of running the analysis to an acceptable level, the local details of the structure must be simplified. As long as the global response of the structure is represented with good accuracy, local details can be excluded and some error in the local behavior of the structure are accepted.

It is therefore important that these simplifications are clear to the user, and that the global model only is used for analysing the global response in the structure. For analyses where the local response is important, a separate model must thus be developed.

7.1.3 Force-indentation Curve

When a ship is colliding with a structure, the forces from the bow on the structure are dependent on the geometry and the structural properties of the bow and the structure. For example; the contact forces are usually high when the bulbous bow is intact, but as it collapses, the forces decrease. Finding this relationship between the forces and the deformation, or indentation, require nonlinear analyses with a large number of elements accounting for plastic deformations. This can not be done in the global analysis and must therefore be done in separate local analyses. The results of these analyses are highly dependent on how the ship bow and the structure are deformed. This will as mentioned in Section 7.1.1 be highly dependent on the strength relations and the geometrical shapes of the ship and the structure. From such analyses it is normal to collect force-indentation curves, where the contact force is plotted vs the indentation.

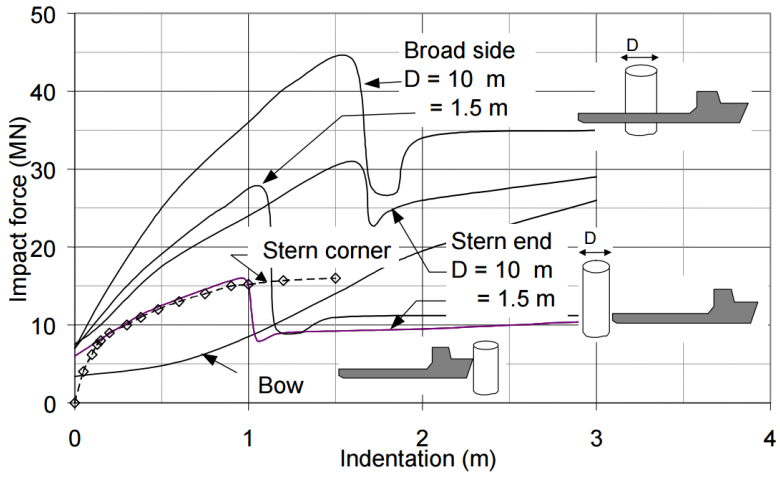

Figure 7.3: Example of force-indentation curve (*NORSOK N-004, Annex A*)

Even though the force-indentation curves are varying between different collisions, NORSOK N-004, Annex A presents standardized force-indentation curves developed for design ships colliding with completely rigid columns of offshore structures. These curves are based on the assumption of having a strength design, since only the ship are experiencing deformations. An example of one of these force-indentation curves are presented in Figure 7.3. These can be used as an approximation when subjecting a global model to a collision force.

7.1.4 Design Load

The information in this section are taken from *Eurocode 1, Part 1.7, Accidental Actions, Background Document*. The Eurocode defines ship impacts as accidental events, meaning 'an actions with low probability, severe consequences of failure and usually of short duration' (*Background Document*, page 5)

The severity of a ship collision is depending on the kinetic energy and structural properties of the ship, and where on the structure it hits. With such a large number of different possible collision events, it is impossible to run analyses of all of them. One should therefore look to identify the events where the combination of probability of occurrence and consequence cause the highest risk for the structure.

Equation 7.2 (Eurocode 1. 1.7 - Background Document, page 36), gives the chance of exceeding the given design load for ship collisions. The design-load can thus be found by inserting the acceptable exceedance probability on the left hand side. It can be seen that the design load will be dependent on a number of parameters like the number of and types of ships, probability of ship failure, among others. It is also seen that the ships position in the fairway, relative to the structure, is of importance. For the prospective floating bridge, the pontoons closest to the navigational channel will probably have the highest design load, since such a collision would require the least deviation from the indented course. The Norwegian Handbook for Bridge Construction allows for an annual exceedance probability bellow 10^{-4}(Andersson, Wilske and Forsman (2016c)), which is governing for the bridge as a whole.

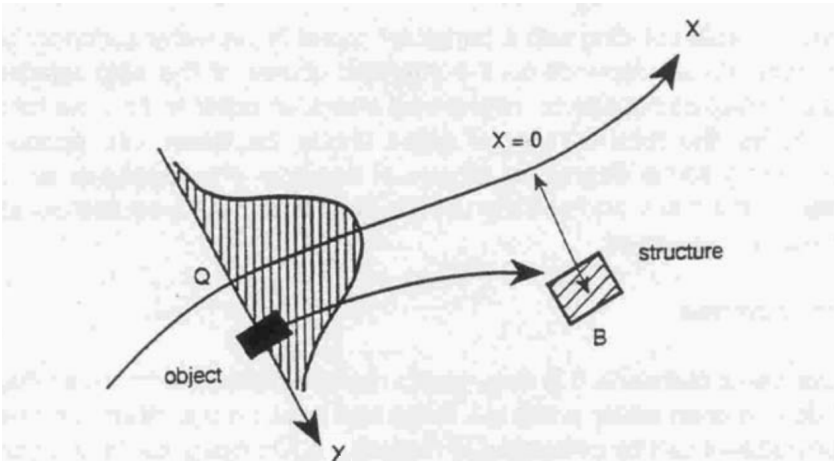

Figure 7.4: Example of distribution of ship traffic passing a structure.(EUROCODE 1)

$$P(F > F_d) = nT(1 - p_a) \int \int \lambda(x) P[v(x,y)\sqrt{km} > F_d] f_s(y)\,\mathrm{d}x\mathrm{d}y \tag{7.2}$$

Where:

T = Period of time under consideration

n = Number of ships per time unit

$\lambda(x)$ = Probability of a failure per unit travelling distance

$P_c(x,y)$ = Conditional probability of collision, given initial position (x,y)

$f_s(y)$ = Distribution of initial ship position in y direction, as seen in Figure 7.4

P_a = The probability that a collision is avoided by human intervention

$v(x,y)$ = Impact velocity of ship, given error at point (x,y)

k = Stiffness of the ship

m = Mass of the ship

7.1.5 Nonlinear and Plastic Analysis

The stress-strain curve for steel is shown in Figure 7.5. The area under the stress strain curve represents strain energy, and as can be seen, the elastic region, represents only a small part of the total elastic energy available. The strain energy being dissipated in ship collisions can be very large, and thus keeping within the linear-elastic region would, at least for the local deformations, be impossible without making the structures highly over-dimensioned. As mentioned in section 7.1.4, ship collisions are defined as accidental events which have low probability of occurrence. As for other ALS events, for the most severe collisions it is acceptable with some damage to the structure, as long as the structural integrity of the superstructure is not lost. Large deformations in the bridge is therefore allowed, and the linear theory is thus no longer sufficient.

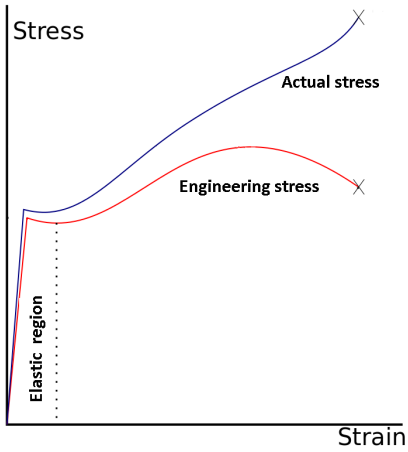

Figure 7.5: Stress-strain curve for steel. Illustration of remaining strength after elastic region (`Wikipedia.com` - stress-strain curve)

7.1.6 Dynamic versus Static Analysis

In the publication *Ship Collision with Offshore Structures* (1993), by By Jørgen Amdahl and Ernst Eberg, the effect of using a dynamical vs a statical analysis model for ship impact on a jacket and a jack up is investigated. It was found that 'the jacket response for the impact scenario considered can be reasonably well predicted by a static approach, because the impact duration is relatively long compared to the fundamental period of the governing motion...' (*Amdahl and Eberg*, 1993). For the bridge considered in this report however, the eigenperiods are much longer than the duration of the collision force, and dynamical effects will be important. It is expected to see the same dynamical effect as described in the publication *Ship Collisions with offshore platforms* (1980), by Olav Furnes and Jørgen Amdahl. 'Some of the impact energy will be transferred into kinetic energy due to excitation of vibrations in the platform. Hence, a static approach may be insufficient in order to determine the energy absorbed in global bending of the platform.'(*Furnes and Amdahl*, 1980). A dynamic time-domain simulation will therefore have to be performed, to correctly represent the physics of the collision problem.

7.2 Work

7.2.1 Ship Traffic and background from Failure Analysis

For the bridge design, a large number of possible ship collision scenarios can occur. To be able to determine what scenarios pose the greatest risk for the bridge, knowledge about the collision energies and what parts of the bridge that are most accident-prone, are important. In the following section, a short overview of the work done on this matter in a collaboration between the Norwegian Public Road Administration(NPRA) and The SSPA are presented, and its meaning for choice of analysis scenarios used in this thesis, are discussed. The information is gathered from Bjøndal, Akhtar, Forsman, Andersson and Wilske (2016a), Bjøndal, Akhtar, Forsman, Andersson and Wilske (2016b) and Andersson, Wilske and Forsman(2015).

The Automatic Identification System(AIS) installed on all ships of significant size, was used to track the ship traffic in the area between 2009 and 2013. The results show that the traffic in the

fjord is dominated by vessels below 100m length, as seen from Figure 7.6.

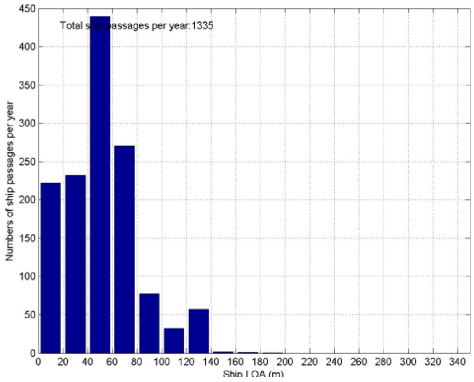

Figure 7.6: AIS data for ship passages into Bjørnafjorden during 2009-2013.(Bjøndal et al. (2016a))

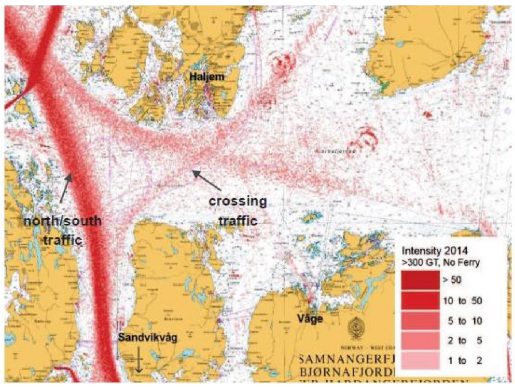

Figure 7.7: Map showing the intensity of ship traffic in the area around the bridge crossing. The ferry traffic, which the bridge will replace, is excluded. (Bjøndal et al. (2016b))

Due to the geography in the area of the crossing, there are a large number of ships passing by the bridge, not entering the fjord, as can be seen in Figure 7.7. This means that the bridge might have to be designed to withstand larger ships than the ones listed in Figure 7.6, which only includes the ships entering the fjord.

To get a good approximation as to what ship energies the bridge should be designed to withstand, the SSPA ran a Monte Carlo simulation for ship accidents in the area (Bjøndal (2016c)). A number of ships was set to follow different expected pathings as seen in Figure 7.8, and at a certain frequency, errors of different nature were introduced, making the ship deviate from the intended course. The frequency of these errors were based on average error rates collected over the Norwegian coast, and included both human and technological errors. The ships were also modeled to try to correct the error trough for example repair or adjustment of course. In the case of an event where an error occurs, and despite correctional actions, the ship collides with the bridge, the collision energy is logged. The simulation was run with the distribution of vessels expected for year 2035, and the number of vessels were 1 million times the expected number of passages per year. In this way, the number of accidental events was high, and the probability of a collision with a certain energy could be found.

In Figure 7.9 the results from the analysis is presented, where each of the dots represents a ship collision with the bridge during the 1 million years simulated. On the y-axis the collision energy is given, and by looking at a certain energy level, and noting how many collisions exceeds this energy level, the annual probability of exceedance can be estimated. The energy level with an annual probability of 10^{-4} is found, and marked with a red line. The annual exceedance probability should be governing for the bridge as a hole, and not per bridge part.

From Figure 7.9 it can be seen that the pontoons closest to the navigational channel, has the highest number of collisions. This indicates that designing the whole bridge to withstand 322 MJ, which gives 10^{-4} annual probability for the entire bridge, might not be the best solution. Instead the energy levels are divided into two parts, as seen by Figure 7.9, where the energy level for the middle part is set to 758.6 MJ and for the rest of the bridge it is 150 MJ. The total exceedance probability for the bridge is still 10^{-4}, but the bridge can be strengthened against ship collisions where most of the collisions will occur.

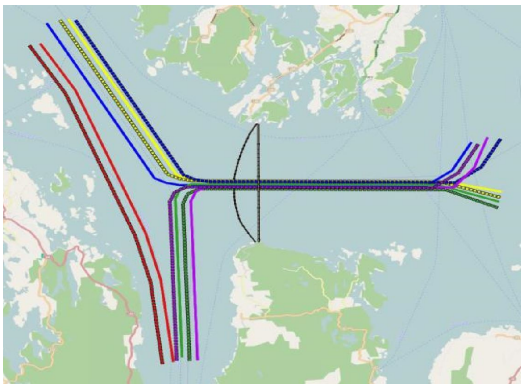

Figure 7.8: Ship paths used in the Monte Carlo simulation by SSPA (Bjøndal et al. (2016b))

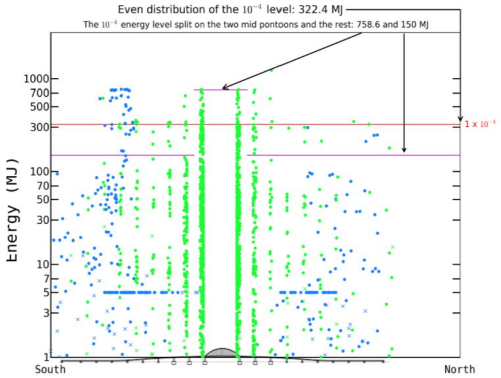

Figure 7.9: Ship collisions with corresponding energies, and positions on the bridge. The blue dots represents collision with the bridge girder, while the green dots represents collision with the pontoons. Red and purple lines have an anual exceedance probability of 10^{-4}. (Bjøndal et al. (2016b))

What will be the design requirements for the bridge is not certain, and when doing the analysis, the bridge will thus be checked against the worst case scenario. This will correspond to using the purple curve for the pontoons next to the navigational channel, while the evenly distributed energy corresponding to the red curve will be used for the rest of the bridge.

The bridge in Figure 7.8 and 7.9 has the navigational channel in the mid section, and it is not the bridge modeled in this Master thesis. A corresponding figure for the bridge with the navigational channel in the south was not presented in the papers, although the analysis were also conducted for this design. The evenly distributed collision energy where however given to be 205 MJ (Bjøndal (2016a)). This is significantly lower than for the bridge in Figure 7.9 for which it was given as 322.4 MJ.

For the bridge analysed in this thesis, one would also want to divide the collision energy into one high energy level over the navigational channel, and a lower level for the rest of the bridge. One would assume that the the 10^-4 energy, both over the navigational channel, and for the rest of the bridge, would be significantly lower for the bridge analysed in this thesis, compared to the one in Figure 7.9. This assumption is based on the fact that the evenly distributed collision energy where significantly lower. However, for a good estimation for the collision energy, one would thus need full access to the results of the analyses performed.

Table 7.1: Collision energies used for collision scenario 1

Collision energies for navigational channel [MJ]	Collision energies for other parts of the bridge [MJ]
500	150
600	250
700	300
800	350
900	400
	450

	MS Color Magic
Tonnage	75,100 GT
Lenght	224 m
Beam	35 m
Draught	6.8 m
Max speed	22 knots(∼11.32 m/s)

Figure 7.10: The ship colour magic (*Wikipedia.com* - Color Magic))

Due to the significant uncertainties connected to the designing(better word??) energy levels, a range of collision energies are used in analyses. By doing this, the effect of a change in collision energy could be seen, as well as choosing the wrong collision energy would be avoided. The collision energies used in the analyses, are presented in Table 7.1, with different values for the pontoons closest to the navigational channel, and for the rest of the bridge.

7.2.2 Design Ship

As was seen in the last section, the analyses will be run for different energy levels due to uncertainty in what collision energy levels the bridge would need to be designed for. In section 7.1.3 it was described how a force indentation curve for the bow, would need to be obtained to run the analysis. For this analysis the curve is obtained from a local bow crushing analysed, which is briefly described in section 7.2.4. For this analysis, a detailed geometry for ship bow would need to be chosen. The ship bow used is not an exact model of any existing ship, but it is a large cruise ship, with geometries similar to the ship MS Color Magic as seen in Figure 7.10.

7.2.3 Global Modeling of Ship Collisions

As mentioned in section, the response of ship collisions rely heavily on the local interaction between the ship and the structure, and this interaction should thus be established through a local analysis. When running the global analysis, these results from the local analysis must be introduced to represent the ship-bridge interaction.

In USFOS, this is recommended done with nonlinear springs, and a point mass with kinetic energy corresponding to the striking ship. An illustration of this analysis process is given in Figure 7.11. The kinetic energy of the ship is introduced through a point mass with an initial velocity towards the structure. Nonlinear springs are used to represent the ship-bridge interaction, and the springs are set to follow the force-deformation curve found from the local bow crushing analysis as described in the previous section. In this way the magnitude of the contact forces would be modeled fairly correctly for each time instant of the analysis.

One could think that it could be an option to introduce the ship collision force as a force with a time history found in the local analysis. The problem with doing so, is that the time history of the force is highly dependent on the structural response. If oscillation in the structure act against the ship, the forces will be large, while as oscillations act together with the ship, the force will be small. The local analysis are done with crushing against a rigid wall and do not

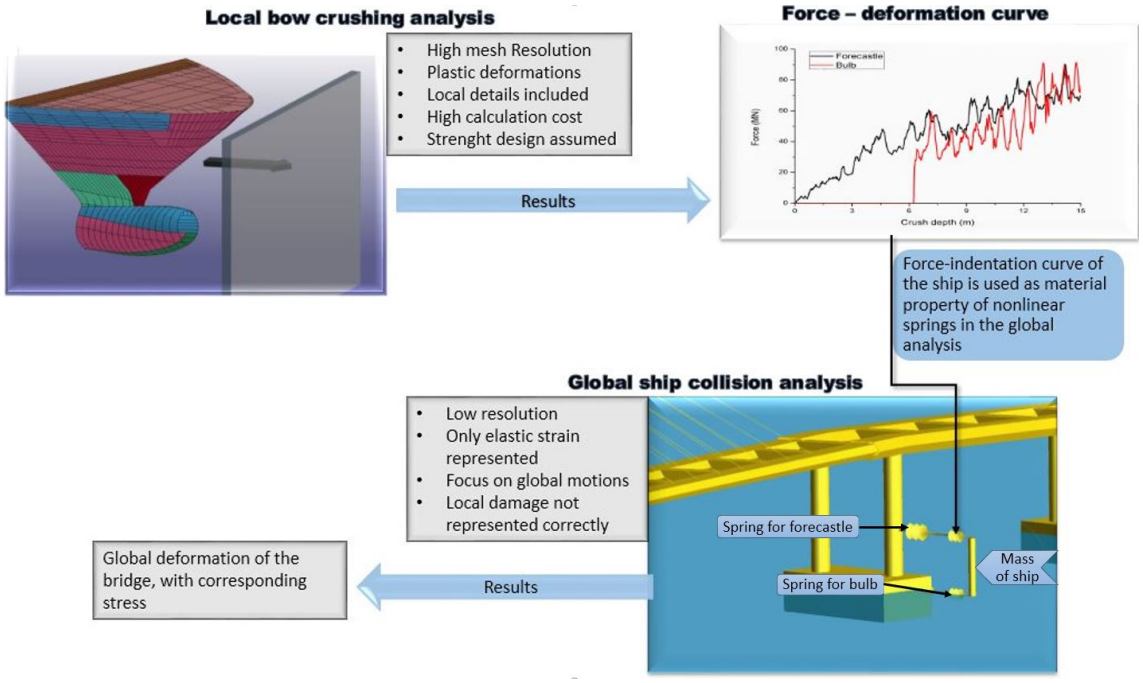

Figure 7.11: Illustration of the process of using nonlinear springs to represent the ship-bridge interaction in a global ship collision analsis

introduce the global response of the structure. The time histories for the force in the local analysis, will thus not be correct for the global analysis. Specific curves for the analysis run in this thesis are given in section 7.2.4.

By introducing the collision force with the mass-spring system described above, one would thus get a much more accurate representation of the collision force. Because the springs force on the structure will depend on the indentation, the structures global response will affect the collision force. In this way both the global and local effects can be represented in the analysis.

Since most of the deformations in the bow during the ship collision are plastic, the spring should not follow the force-deformation curve, during the unloading of the collision force. It should follow the collision curve as long as the spring is being compressed, but when the spring start to extract, the ship should be detached. To simulated this, another spring is added in series with the nonlinear spring. By giving this spring a very high stiffness in compression, and a very low stiffness in tension, only the forces acting during the unloading would be negligible.

7.2.4 Local Bow Crushing Analysis in LS-Dyna

As mentioned previously, a force indentation curve is needed to represent the bow-bridge interaction, when running the ship collision analysis in USFOS. A bow crushing analysis to obtain this curve was run by post doc Yanyan Sha with a ship model developed by Master Ole Harald Moe. The ship model used was a large cruise ship, as described in section 7.2.2. The analysis was run in LS-Dyna, and with the proper representation of local details and the programs abilities to model plastic deformations and surface contact accurately, the physics of the bow crushing is very well represented.

The force deformation curve is found by running the ship model into a rigid wall at small distance increments, measuring the contact force from the bow onto the wall. The forces are

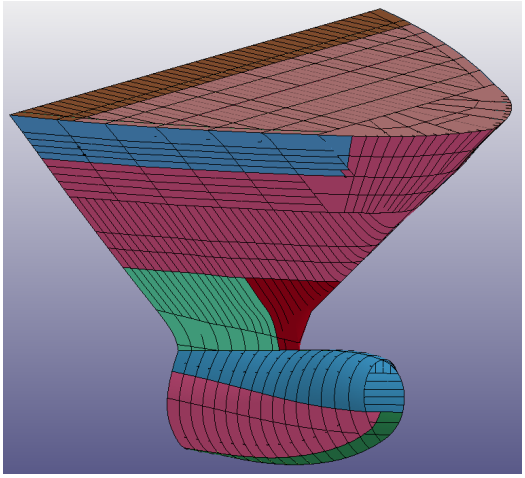

Figure 7.12: Model used in LS-Dyna analysis. (Developed by Post doc. Yanyan Sha and Ole Harald Moe)

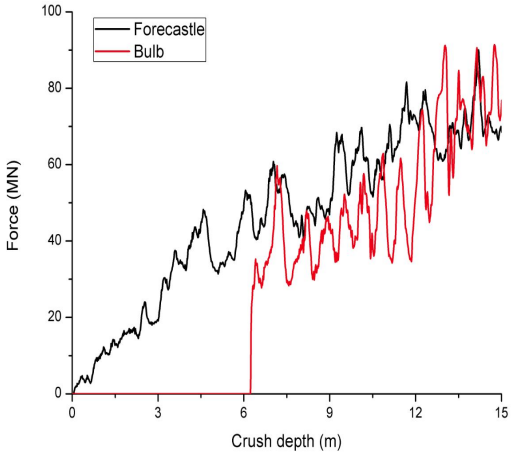

Figure 7.13: Force deformation curve From LS-Dyna analysis. (Developed by Post doc. Yanyan Sha and Ole Harald Moe)

divided into two different curves as seen in Figure 7.13, one representing the bulbous bow, and one for the forecastle. The forces for each will thus be applied as two different springs in the USFOS model, as can be seen in Figure 7.11.

The force-deformation curve was found by crushing the bow against a rigid wall, where the wall experience no deformations. This corresponds to a strength analysis, as described in Section 7.1.1. If the real ship-bridge interaction differs a lot from this assumption, by the bridge experiencing large local deformation, the force-deformation curve will not be a good representation of the ship collision force.

It is thus assumed that the local strength of the bridge is sufficient in the scenarios investigated in this thesis. The validity of this assumption should be checked with local collision analyses, but this will not be done in this Thesis. In Section 8.4.7 however, the effect of local damage on the global strength of the structure is discussed briefly.

The force-deformation curve found are also greatly affected by the geometry of the rigid structure the bow is crushed against. For the curves to be good representations for the ship-bridge interaction, the geometry of the bridge should thus not differ greatly from the rigid wall used in the LS-Dyna analysis.

7.2.5 Collision Scenario 1

In this scenario, the ship is colliding with the column closest to the navigational channel, and the ships heading is along the navigational channel, colliding into the short edge of the pontoon.

By looking at the geometry of the ship, and the pontoon in Figure 7.14, it can be seen that the first point of impact would be at the bulbous bow when colliding into the pontoon. It is also possible for the forecastle of the ship to hit the front column of the pontoon. For this to happen the collision must inhere enough energy to first crush 5.27 meter of the bulb.

This collision scenario is represented by two series of springs, one representing the bulbous bow and one representing the forecastle, as can be seen in Figure 7.15. The springs are given the force-deformation curves found in the local bow crushing analysis as described from Section

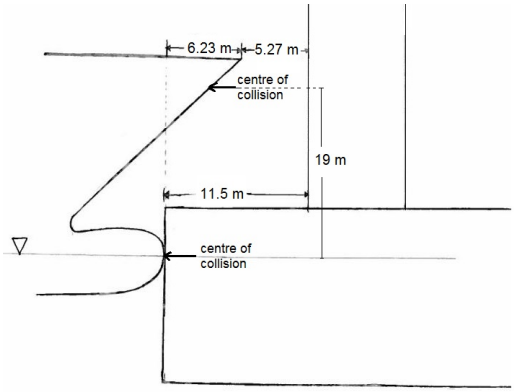

Figure 7.14: Illustration of the ships collision with the pontoon and column, with important dimensions given

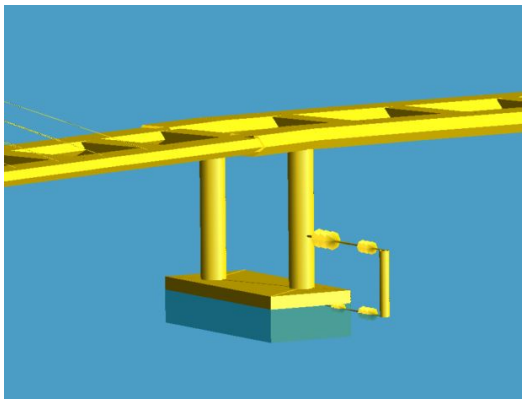

Figure 7.15: Illustration of how the system of springs are introduced in the Usfos model, to represent the ship collision force in collision scenario 1.

7.2.4. The Usfos software has a limit on the maximum number of data points that can be used in this curve, and simplification of the curve must be made, where some of the details are excluded. These simplified curves are presented in Figure 7.16 and 7.17, and it is seen that despite the simplifications, it represents the stiffness of the bow fairly accurately.

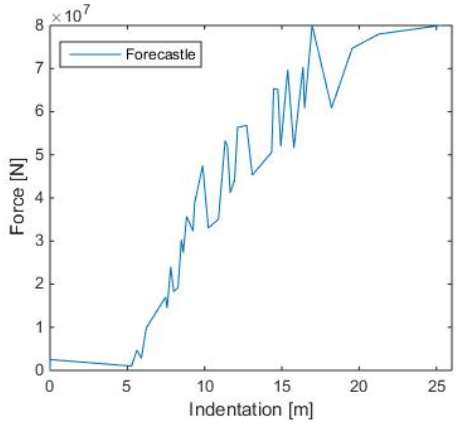

Figure 7.16: Force indentation curve used to represent the ships forecastle. (The first 5.27 meter of the curve are set to a small value, and not zero, because this would cause the analysis to crash)

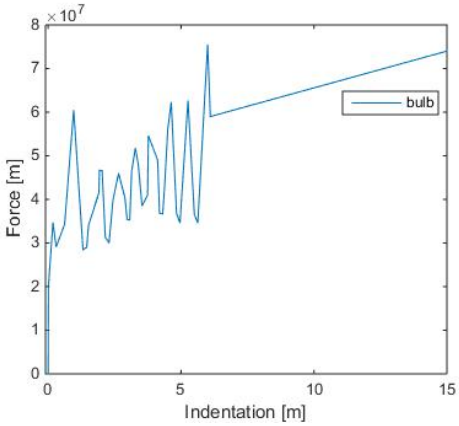

Figure 7.17: Force indentation curve used to represent the ships bulb

The position where the springs are attached are determined from what is expected to be the centre of the collision force for each part. This position will change depending on how much of the ship that is crushed. The inclination of the bow will for example make this point move downwards as more of the lower parts of the forecastle contribute to the contact forces. Since the analysis is run with differing collision energies an exact position can not be found, but a rough estimate based on the assumed bow deformation is set, as seen in Figure 7.14. Even with an error in the order of a meter, the effect on the global results will be minor. The height might affect the pendulum motion of the pontoon in a small degree, but this will have less effect on the bending of the bridge girder.

The mass of the ship is evenly distributed with half the value at the end of each spring. It is natural to assume that the forecastle and the bulbous bow, will move as one rigid body. It is thus not acceptable having the springs compressed at different speeds due to the difference in stiffness. The springs are thus connected with beam with artificially high stiffness, keeping the indentation of the two springs equal. Since the indentation of the spring for the bulb and the forecastle will be equal at all times, the force-indentation curve of the forecastle must be altered in such a way that the collision force is not introduced before 5.27 meters of the bulb are crushed. The force deformation curve of the bulb is thus shifted along the x-axis, giving zero force until a crush depth of 5.27 meters, while the force from the bulb contribute immediately. The force deformation curves in Figure 7.16 and 7.17 thus differ from the bow crushing analysis presented in Section 7.2.4, where the first collision occur at the forecastle.

As discussed in Section 7.2.1, the collision energies the bridge should be designed against are not known yet. Based on the discussion presented in that section, a number of different collision energies were used for this collision scenario, and are provided in table 7.2. The energies are altered by changing the mass if the ship, while the ships collision speed is kept constant, at 5 m/s or 9.72 knots. This value is chosen because there have been suggested to introduce a speed limit in the order of 10-12 knots for the area around the bridge (Bjøndal et al.(2016a), page 32).

Table 7.2: Collision energies used for collision scenario 1 and 2

Collision energy [MJ]	Ship speed [m/s]	Ship speed [knots]	Ship mass [ton]
500	5	9.72	40 000
600	5	9.72	48 000
700	5	9.72	56 000
800	5	9.72	64 000
900	5	9.72	72 000

7.2.6 Collision Scenario 2

In this scenario, the ship is again colliding with the column closest to the navigational channel, but the ships heading is now transverse of the direction of the navigational path. The ship is thus colliding into the long end of the pontoon. The ship is set to hit in the middle of the pontoon, and thus the forecastle will not hit any columns, and only the bulb will contribute to crushing stiffness.

The ship is thus represented by only the spring for the bulb, with the force deformation curve given in Figure 7.17. The total mass of the ship is thus concentrated at the end of this spring, instead of being divided between two nodes with the rigid beam as a connection.

The analysis on the ship collisions energies presented in Section 7.2.1 does not distinguish between a collision into the short side of the pontoon and in the long side. The collision energy giving the 10 000 year limit, is thus the same regardless of where on the pontoon the ship hits. The analysis is thus run for the same collision energies as collision scenario 1, even though the probability for high energy collisions most probably would be higher in the direction of the navigational channel.

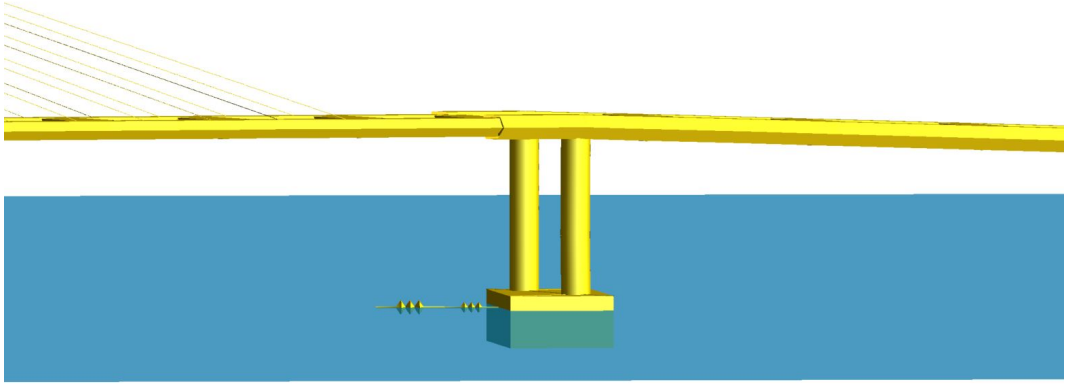

Figure 7.18: Illustration of the springs used to model the collision force from the bulb onto the pontoon for collision scenario 2

7.2.7 Collision Scenario 3

In this scenario, the ships forecastle is colliding directly into the bridge girder, as seen in Figure 7.19. For the parts of the bridge closest to the navigational channel this is not possible due to the height of the bridge. However, when moving away from navigational channel, the bridge will descend reducing the air-gap under the pathways. At the position of the impact in this collision case, the height of the center-line of the bridge girder is 18.16 meter. The height of the ships forecastle is 22 meter and would thus not be able to pass under the bridge, and a collision will occur. Due to the height of the bridge girder, and absence of pontoons at the point of impact, the bulb will pass under the bridge, and not contribute in the collision.

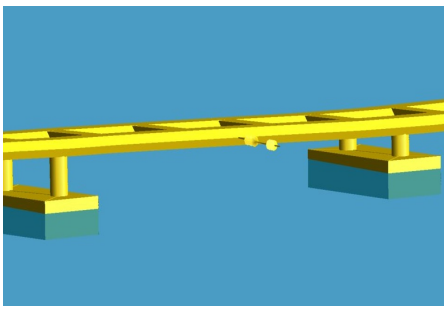

Figure 7.19: Illustration of the springs used to model the collision force from the forecastle onto the bridge girder for collision scenario 3

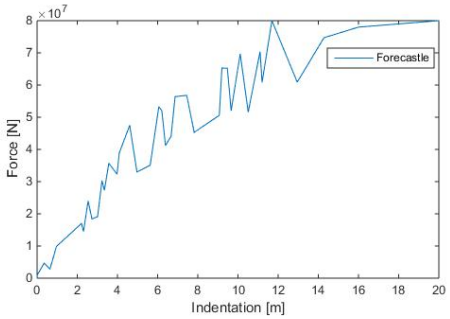

Figure 7.20: Force indentation curve used to represent the ships forecastle

As discussed in Section 7.1.6, the designing collision energies will be lower for this part of the bridge, since it is further away from the navigational channel. It should be able to absorb 322 MJ if the deign criteria is set as a mean value over the whole bridge, and if it is divided into several values, it would be even lower. As discussed, these values are still associated with significant uncertainty, and several collision energies, as presented in Table 7.3 are thus investigated in the analysis.

The ship is again modeled with a spring with the force deformation curve of the forecastle from the bow crushing analysis, but opposed to collision scenario 1, the curve starts increasing at zero deformation, as seen in Figure 7.20.

Table 7.3: Collision energies used for collision scenario 3

Collision energy [MJ]	Ship speed [m/s]	Ship speed [knots]	Ship mass [ton]
150	5	9.72	12 000
250	5	9.72	20 000
300	5	9.72	24 000
350	5	9.72	28 000
400	5	9.72	32 000
450	5	9.72	36 000

7.3 Results

The response of the bridge are described and illustrations from Usfos are in this section presented to give an impression of the structural response from each collision case. For the response to be easily observed, the displacements are scaled to a number of times the actual displacements. This scale factor is presented in the figure descriptions, and the figures are showing an exaggeration of the structural response. To keep the number of figures to a minimum, only illustrations of the most important response is presented, and a throughout presentation of the whole response history would not made. For a more extensive response history, animations of the response will have to be investigated. These will however not be presented in this report, in order to protect the work from plagiarism.

In addition to the displacement response, the locations with the most critical stresses are found, and the plastic utilization is presented. For the parts where the initial stresses are assumed to be wrong, the increase in plastic utilization are instead presented, as explained in Section 3.4. No criteria were through the work with this thesis found with regards to acceptable accelerations in the pathways. However, the maximum observed accelerations are included, since this would pose a significant threat to possible traffic on the bridge during the collision. This is discussed briefly in Section 8.4.6

7.3.1 Collision Scenario 1

The response of the bridge after impact consists mostly of a combination of bending of the bridge girder in the x-direction, and pendulum motion of the pontoon, causing twisting of the bridge girder. The twisting starts locally with just the pendulum motion of the struck pontoon, as is seen in Figure 7.21, where-after twisting spreads to include more of the pontoons in a more global mode, like shown in Figure 7.22.

A similar response is seen for the horizontal displacement in the direction of the collision. A local bending mode develop rapidly at the point of impact as shown in Figure 7.23, while a more global mode develops over time, as the displacement spreads out over the bridge length. This deformation spreads like a wave throughout the bridge, until a more or less global mode is achieved. When the wavefront of the bending mode reaches the end of the bridge, a reflecting of the wave can be observed.

The bending stresses observed in the bridge is highly dependent on the curvature of the bridge. The most critical stresses are thus observed during the more local bending modes, where the bending energy is concentrated in local flexing of the beam. As times goes by, the bending

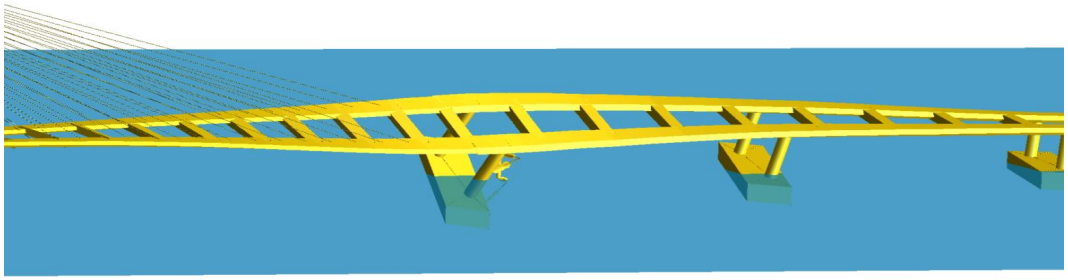

Figure 7.21: Deformation of bridge after 23 seconds, showing a local twisting mode. Deformations scaled by a factor of 10

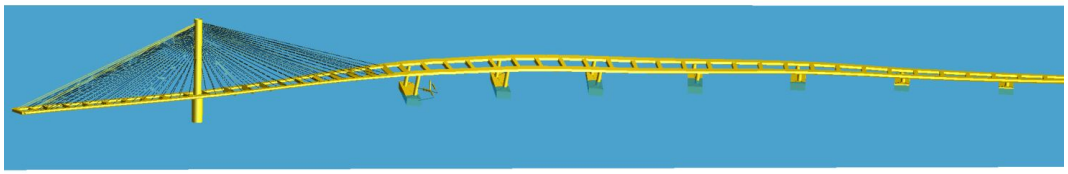

Figure 7.22: Deformation of bridge after 32.68 seconds, showing the development of a more global twisting mode. Deformations scaled by a factor of 10

energy spreads out throughout the bridge, giving larger overall deformations, but smaller values for the concentrated stresses. The effect of the wavefront of the bending modes being reflected when reaching the fixed boundary conditions at the end of the bridge, will thus not be important for the occurrence of high plastic utilization in the bridge. The most critical values occur shortly after impact.

The most crucial points with regards to plastic utilization, and which is investigated during the analyses are marked in Figure 7.24. On the bridge the most critical point is at the column connection, marked as critical point number one in Figure 7.24.

As was discussed in Section 3.4 - The wires for the cable-stayed bridge are intended to be pre-tensioned, to support the weight of the bridge girder. In USFOS, such a pre-tension is not possible to model properly and the initial stresses in the bridge girder for the cable stayed section, are thus modeled incorrectly. The results found are thus given as the increase in plastic utilization instead of the value of the utilization factor. It is important to note that the increase is given with relation to the utilization factor connected with the real yield stress of the material, where a utilization factor of 1 corresponds to plastic deformations. The increase given are thus twice the increase found in the analysis, where a plastic utilization factor of 0.5 would give plastic deformations in the real structure.

At the connection between the bridge girder and the cable tower the plastic utilization is very high initially. Due to the error in the initial stresses, as was just discussed, this is most probably not a realistic stress level. However, it is not certain how much lower the stress in reality would be. In case the real stress should also show to be high for this position, the increase in plastic utilization is checked at this point, even though the increase are expected to be low.

The values for the maximum increase in plastic utilization for point 1 and 2 are presented in

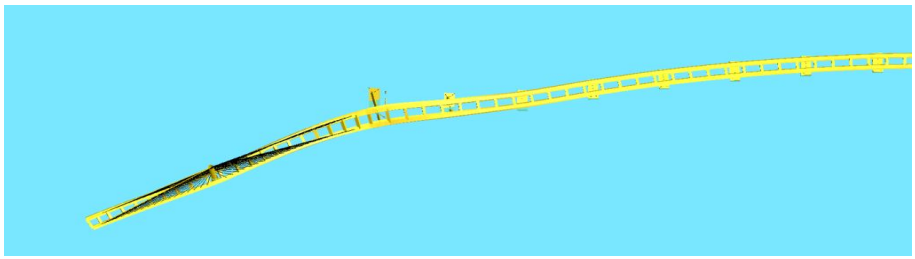

Figure 7.23: Deformation of bridge after 22.85 seconds, showing a local horizontal bending mode. Deformations scaled by a factor of 20

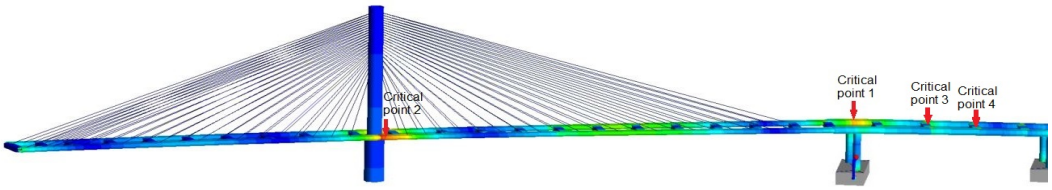

Figure 7.24: Most critical points with regards to plastic utilization for collision scenario 1

Table 7.4 for the different collision energies.

Table 7.4: Maximum increase in the plastic utilization of the bridge girder, given for different collision energies investigated

Collision energy [MJ]	Increase in plastic utilization at point 1	Increase in plastic utilization at point 2
500	0.468	0.082
600	0.488	0.098
700	0.470	0.106
800	0.484	0.110
900	0.486	0.116

Also the cross-beams between the bridge girders experience large stresses that results in a high plastic utilization. The beams with the highest utilization is the second and third beam away from the point if impact. The maximum plastic utilization is thus collected from these cross beams, in what is marked as critical point number 3 and 4 in Figure 7.24. For these points it is sufficient to find the total plastic utilization, and the increase is of less interest. Table 7.5 presents the maximum plastic utilization in point 3 and 4, for the different collision energies.

Although the plastic utilization is the most interesting result when assessing whether the structure would survive the collision without critical damage, other results can also be of interest, as was previously mentioned. In Table 7.6, the maximum horizontal displacement of the bridge girder at the position of impact are given, together with the maximum observed vertical and horizontal accelerations of the pathway.

As explained previously, the response shortly after the impact is the most critical for discussion around the bridges strength against ship impacts. The later time-history of the response are not presented in the report in a lucidly manner.

However, the deformation history of the horizontal displacement of the bridge girder at the point of impact, are presented in Figure 7.25, giving an inpression of how the response of the

Table 7.5: Maximum values of the plastic utilization of the cross beams, given for different collision energies investigated

Collision energy [MJ]	Plastic utilization at point 3	Plastic utilization at point 4
500	0.884	0.841
600	0.862	0.858
700	0.881	0.881
800	0.895	0.892
900	0.904	0.905

Table 7.6: Maximum values for the deformation in x-direction, and the accelerations in x and z direction, for the point in the bridge girder, just above the struck pontoon

Collision energy [MJ]	deformation [m]	horizontal acceleration [$\frac{m}{s^2}$]	vertical acceleration [$\frac{m}{s^2}$]
500	4.58	2.74	1.24
600	5.27	2.74	1.24
700	5.88	2.74	1.24
800	6.57	2.74	1.24
900	7.16	2.74	1.24

bridge vary over time. A collision energy of 900 MJ was used for the analysis of the displacement history presented. Note that the deformation history confirms that the most extreme response is seen shortly after the impact introduced after 20 seconds

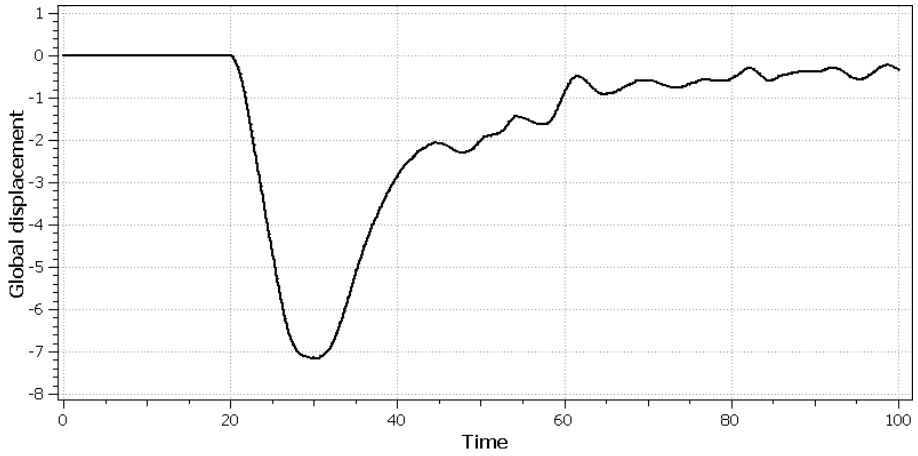

Figure 7.25: Time history of horizontal displacement of bridge girder at position of impact, for a collision energy of 900 MJ, in collision scenario 1

7.3.2 Collision Scenario 2

The response of the bridge after impact is dominated by a pendulum motion of the pontoon in the direction of the impact. Due to the rigid connection between the column and the bridge girder, this pendulum motion induce a vertical bending in the bridge girder, as seen in Figure 7.26.

The pontoons are oriented along the x-axis, while due to the curvature of the bridge, towards the ends of the bridge, this will not be perpendicular to the longitudinal direction of the bridge.

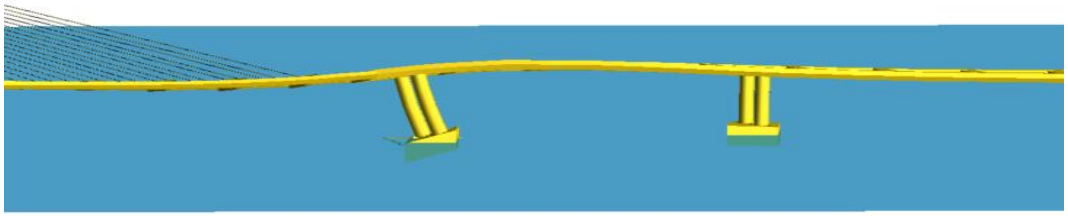

Figure 7.26: Deformation of bridge after 21.83 seconds, showing a local beding of the bridge girder, due to pendulum motion of the pontoon. Deformations scaled by a factor of 10

Since the collision force do not act perfectly along the longitude of the bridge, the impact would also result in a pendulum motion in the x direction causing a twisting of the bridge girder, as shown in Figure 7.27.

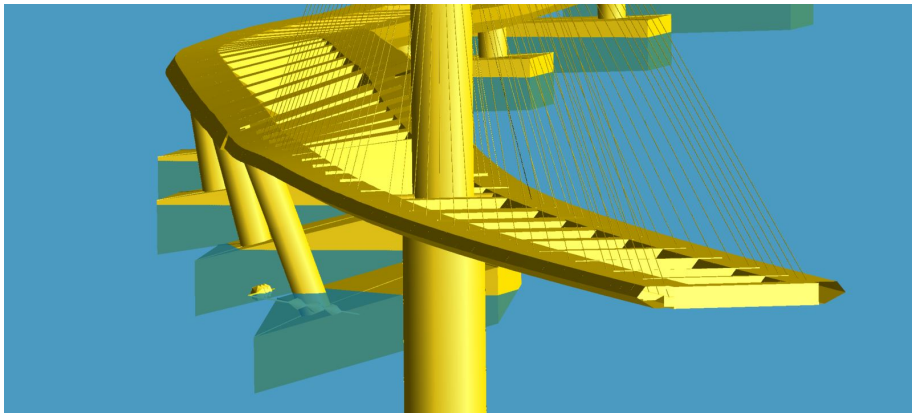

Figure 7.27: Deformation of bridge after 27.2 seconds, showing the twisting og the bridge girder developing into at more global mode. Deformations scaled by a factor of 5

In conformity with what was observed for collision case 1, the response starts as a local mode, that over time develops into a more global response that include larger parts of the bridge. The local modes give larger stress concentrations, and the maximum plastic utilisation is thus found few seconds after impact.

The most critical points on the bridge with regards to the plastic utilization are shown in Figure 7.28. It is seen that the pendulum motion of the pontoon introduce large bending stresses in the bridge girder at point 1 due to the rigid connection between the girder and the column. This connection also give large stresses in the the top of the column at point 3. As discussed in case 1, also the utilization increase at point 2 are checked despite the fact that the utilization increase are expected to be low.

The maximum utilization increase for point 1 and 2 are presented in Table 7.10, While for point 3 at the column, the maximum plastic utilization are the property investigated, and presented in Table 7.8.

As was done for case 1, also the maximum observed vertical and horizontal acceleration of the pathway is found, together with the maximum vertical displacement of the pathways. The vertical displacement are the largest for node 122 where the deformation has a contribution from both the twisting and the bending of the bridge girder. The results are presented in Table

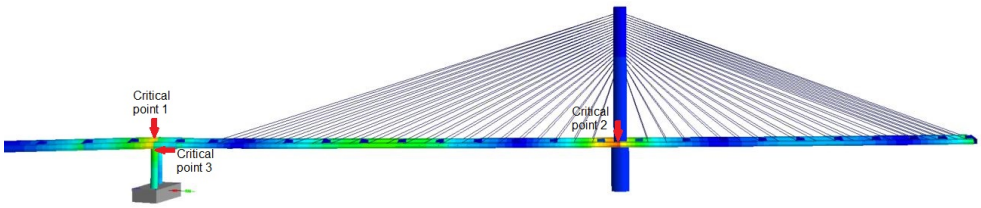

Figure 7.28: Most critical points with regards to plastic utilization for collision scenario 2

Table 7.7: Maximum values of the increase in plastic utilization in the bridge girder, given for the different collision energies investigated

Collision energy [MJ]	Increase in plastic utilization at point 1	Increase in plastic utilization at point 2
500	0.616	0.036
600	0.618	0.032
700	0.624	0.026
800	0.626	0.03
900	0.656	0.072

7.11.

As for case 1, the deformation history is given for the bridge in Figure 7.29. The vertical displacement of node 122 are plotted, to give an insight to how the response of the bridge vary over time. A collision energy of 900 MJ was used for the analysis of the displacement history presented.

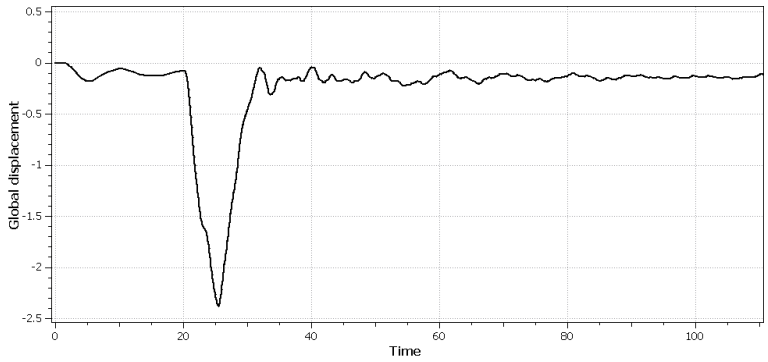

Figure 7.29: Time history of vertical displacement of node 122 for a collision energy of 900 MJ, in collision scenario 2

7.3.3 Collision Scenario 3

The response of the bridge is dominated by horizontal bending of the bridge. Also some minor twisting of the bridge girder are observed, as the struck pathway is lifted upwards while the other pathway moves down. This twisting is most likely due to the pontoons resistance against the motions.

Table 7.8: Maximum values of the plastic utilization in the column at critical point 3, given for the different collision energies investigated

Collision energy [MJ]	Plastic utilization in column
500	0.992
600	0.999
700	1.000
800	1.000
900	1.000

Table 7.9: Maximum values for the deformations and accelerations in the bridge girder, above the struck pontoon

Collision energy [MJ]	deformation [m]	acceleration node 137 [$\frac{m}{s^2}$]	acceleration [$\frac{m}{s^2}$] node 124
500	-1.67	1.37	-1.55
600	-1.85	1.37	-1.55
700	-2.03	1.37	-1.55
800	-2.23	1.37	-1.55
900	-2.37	1.37	-1.55

The horizontal bending starts locally with bending of the bridge girder between the two closest pontoon, as seen in Figure 7.30. Over time the curvature spreads out throughout the bridge, and more global bending modes are observed, as seen in Figure 7.31.

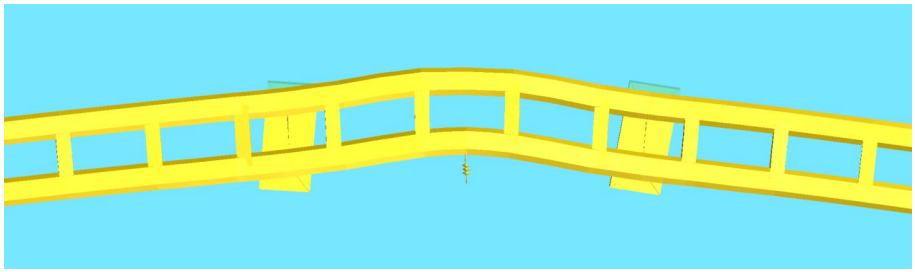

Figure 7.30: Deformation of bridge after 21.79 seconds, showing a local bending mode. Deformations scaled by a factor of 25

Also for this collision case, it is the local bending modes with a sharp curvature that give rise to the highest stresses, and the highest plastic utilization factors are thus found during the development of this modes, shortly after impact.

Figure 7.32 shows the most critical positions with regards to plastic utilization factors. The local bending mode are seen to induce large stresses in point 1, 2 and 3. In point 4, the stresses observed in the column, are due to inertia forces in the pontoon, as it is set into motion.

Note that since this collision case is far away from the cable-stayed section, the value of the plastic utilization are investigated, also for the bridge girder, instead of the utilization increase, as was done for collision scenario 1 and 2.

The plastic utilization for all the points in Figure 7.32 are found for all the different collision energies and presented in Table 7.10.

The maximum observed vertical and horizontal acceleration of the pathway is found, and presented in Table 7.11, together with the maximum vertical displacement. Since the ship

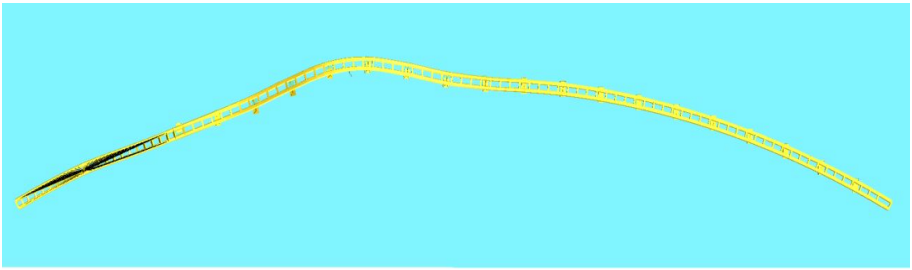

Figure 7.31: Deformation of bridge after 24.12 seconds, showing a more global bending mode. Deformations scaled by a factor of 25

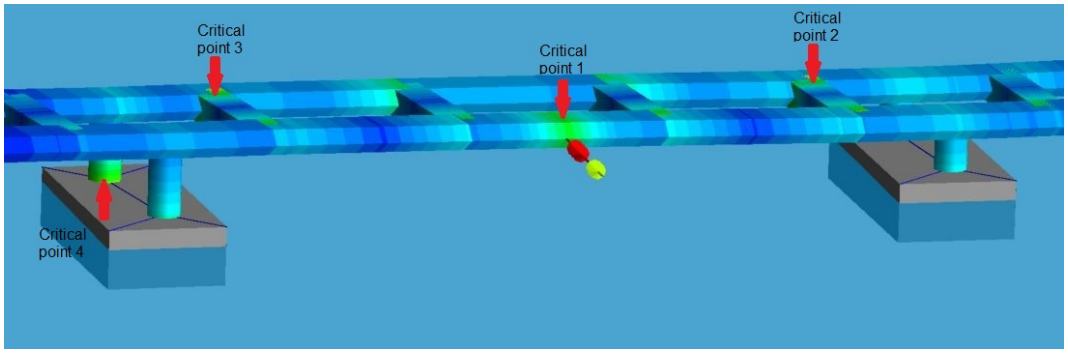

Figure 7.32: Most critical points with regards to plastic utilization for collision scenario 3

collides directly into one of the pathways, it is easily seen that the most critical values would occur at the position of the impact.

It is seen that the accelerations found are extremely high, especially in the x-direction. This is probably due to the fact that the collision force is applied directly to the node where the accelerations are collected. The goodness of these results might thus be questionable, as will be discussed further in Section 8.4.6.

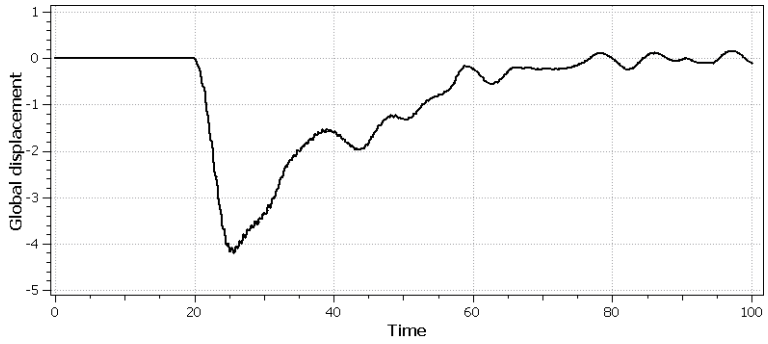

Figure 7.33: Time history of horizontal displacement of bridge girder at point of impact, for a collision energy of 900 MJ, in collision scenario 3

The horizontal displacement on the other hand are probably better represented by the model, and as was done for collision case 1 and 2, the displacement history for this point are included, to give an impression of how the response varies over time. The response history is shown in Figure 7.33, and is from a collision with 450 MJ collision energy.

Table 7.10: Maximum values of the plastic utilization for all the critical points, given for the different collision energies investigated

Collision energy [MJ]	Plastic utilization at point 1	Plastic utilization at point 2	Plastic utilization at point 3	Plastic utilization at point 4
150	0.407	0.515	0.482	0.524
250	0.496	0.705	0.731	0.555
300	0.516	0.783	0.742	0.569
350	0.533	0.810	0.721	0.579
400	0.527	0.786	0.701	0.576
450	0.506	0.763	0.707	0.569

Table 7.11: Maximum values for the displacements and accelerations of pathways. Collected in bridge girder at the point of impact

Collision energy [MJ]	horizontal displacement [m]	horizontal acceleration [$\frac{m}{s^2}$]	vertical acceleration [$\frac{m}{s^2}$]
150	1.56	42.24	1.20
250	2.51	33.83	2.28
300	3.09	30.94	2.40
350	3.41	30.45	2.70
400	3.77	30.64	3.23
450	4.20	30.83	2.17

Chapter 8

Discussion

8.1 Goodness of Model

8.1.1 Over-dimensioned pontoon volume

In Section 3.2.2 it was seen that the volume of the pontoons was over-dimensioned due to the software being unable to model the curved edges. The increase in the buoyancy caused by this error will have two main effects. The stiffness in heave from the water-plane will be too high, which would give a minor effect on the the vertical eigenmodes in the eigenvalue analysis. The main ship collision analyses however, would not be affected much, since the surge, sway, roll and pitch motions are the most important for the response. This water-plane stiffness for these pontoon motions are as seen in Section 3.2.3 introduced by springs, and will thus not be affected.

More importantly the error in buoyancy would influence the amount of ballast added to the pontoon, as found from the ballasting analysis in Section 4. By having an over-dimensioned buoyancy, the weight of the ballast found, would be too high. This weight, would increase the inertia of the pontoons, which will have a great impact on the response from the ship impact. The more inertia inhered by the pontoons, the more energy would be needed to set it into motion during the collision. The increase in volume are below 10 percent, which means that the error is not critical for the results, although it is an error worth noticing.

8.1.2 Added Mass of Pontoons

As described in Section 3.2.5 the added mass in surge, sway and heave for the pontoons are introduced as a property of the beams connecting the nodes at the bottom of the columns. The added mass specified is thus assigned to the local axis system of this beam, and as can be seen from Figure 8.1, this does not always concur with the axis system of the pontoon. Because of this, the added mass introduced in surge and sway will have an orientation differing slightly from the orientation of the pontoon. The direction difference, illustrated by the angle α, is however small for most parts of the bridge, and for the middle pontoons, the direction will be correct. The error increases when moving towards the sides of the bridge, due to the curvature of the bridge, and the pontoon in Figure 8.1 is the worst case. For collision scenario 1 and 2 this is the pontoon struck, and the orientation error could have a minor impact on the results.

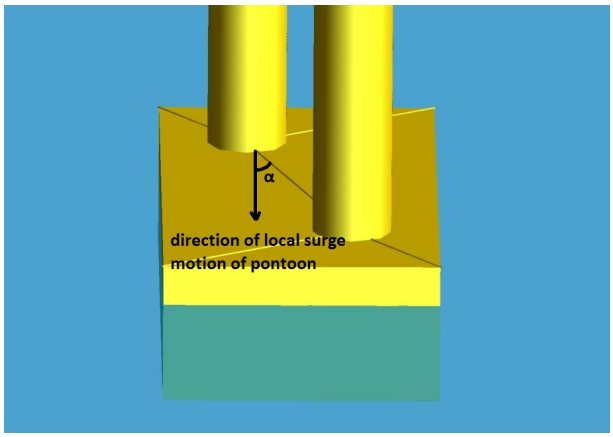

Figure 8.1: Illustration of how the direction of the added mass introduced is incorrect for some of the pontoons. α is the angle between the actual direction of the surge motion of the pontoon, and the local x direction of the pontoon, which is the direction the surge added mass is prescribed to in USFOS.

When choosing the value for the added mass, the values for oscillations above 20 seconds were chosen. From the results of the ship collision analysis, it is however not clear if this was a safe assumption for all of the collision scenarios. In Figure 8.2 the displacement in the sway direction of the struck pontoon is given for collision scenario 2. Shortly after the collision occur, at 20 seconds, the displacement is seen to increase very gradually following the on-loading of the collision force. Little dynamical motions seem to occur at this time instant, the response is almost at static equilibrium with the collision force. The assumption of long oscillations periods can thus be seen as fairly good. However, as the maximum displacement is reached, the response show indications of smaller oscillation periods. It is thus hard to give a conclusion to if the assumption of long oscillation periods for the added mass, is a good assumption or not, and further investigations are advised. For the pontoon motions in collision scenario 1 a similar behaviour is observed.

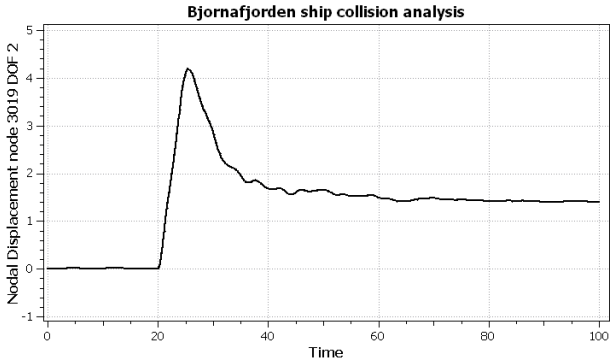

Figure 8.2: Displacement history for the struck pontoon in the sway direction for collision scenario 2.

No added mass is introduced for the rotational degrees of freedom. The response from collision scenario 1, presented in Section 7.3.1, includes a significant pitch motion. The lacking added mass in this degree of freedom could thus give a notable error in the pitch motion of the response, due to a too small rotational inertia.

8.2 Assumptions in Relation to Damping

In Chapter 6 the effect of both the hydrodynamical and structural damping levels are investigated. Different damping levels are used when running collision scenario 1 for a collision energy of 1250 MJ, and the effect on the result of the analysis are presented.

It was found that even with large changes in the damping level, the effect on the maximum displacement and change in plastic utilization were small. Only in the order of a few percent. This indicate that the large focus on determining the right damping level for the structure, were less important that thought initially.

For the exact analyses performed in this thesis this might be the case, however, it is important to note that this might not be the case for all collision scenarios. For the collision scenarios investigated, the early part of the on-loading of the collision force, are happening very gradually, not being affected much by the dynamical response of the structure, as is discussed in Section 8.4.2. The maximum responses both with regards to plastic utilization and deformations, are also occurring shortly after impact. Because of little motions and oscillations are present before the occurrence of the most critical response, the damping will have little effect on the results.

If, for another collision scenario, the most critical response occur at a later time instant, where more dynamical motions have had the time to act, more energy would most likely have been absorbed by damping. Errors in the damping level will thus in such a case, have a greater impact on the results, than what was observed in this analysis.

From the collision scenarios analyzed in this Thesis, it seems to be a reoccurring trend, that the most critical structural response and stresses occur shortly after impact. As the collision energy spreads out through the bridge as potential bending energy, the stress become less concentrated. No indications are found to how the dynamical response could induce critical stresses at later instances.

Developing better estimations for the damping levels would however be necessary for running good analyses on the response to environmental loads at a later stage of the design process. Investigations with relation to the damping are thus advised, despite the effect of the damping on the ship collision analysis, appear to be low.

8.3 Eigenvalue Analysis

From the eigenvalue analysis only the first 20 eigenvalues are included in the report. This is because the model used gives poor accuracy for the eigenvalues below that. These modes have mainly local motions, including rotations of the pontoons. When creating the model, the focus was on giving an accurate result for the global response of the bridge subjected to a ship collision. Simplification where thus made for local details, and the local modes is not modeled correctly by the model. Additionally, the calculation method introduces inaccuracies that become large for the smaller eigenmodes.

To control the results of the eigenvalue analysis, the results are compared to the eigenvalues given in COWI et al. (2016, Appendix E). These were calculated using the software Orcaflex, but besides that, no info on the modeling is given. The accuracy of this analysis is thus not known, and it can thus not be treated as the sole answer, but it can provide an indication to whether the results are reasonable or not. The results given are found in the Appendix in

section 10.2.2, and it can be seen that the results are very similar to what was found through the USFOS analysis. The eigenvalues are however a few seconds shorter than the eigenvalues found in USFOS. A possible explanation of this can be the way the pontoons are modeled in USFOS, giving a to large mass, as discussed in Section 8.1.1.

By not modeling the rounded edges of the pontoons, the pontoons buoyancy will be too large, which trough the ballast balancing, will cause the weight of the pontoons to be to large. This increase in mass, will explain the increase of the eigenvalues, but since little information is given about the Orcaflex analysis, other factors may also cause this difference.

8.4 Ship Collision Analysis

8.4.1 Goodness of Force-indentation Curve

As mentioned in Section 7.2.4, the geometry of the bridge at the point of impact should not differ greatly from the rigid wall used to develop the force deformation curve. If this assumption is good for the collision scenarios in this thesis will be discussed in this section.

For collision scenario 1 from Section 7.2.5, the bulb collides with the pontoon, and the forecastle with the column. The pontoon have a width of 28 meter which is much larger than the bulb, and the assumption of a plane wall is thus good even after several meters of the bulb is crushed. The column however only have a diameter of 8 meters, which is the width of the forecastle after crushing only 4 meters. It is thus unclear, if the force-deformation curve used in the analysis is a good representation of the bow-column interaction. This will depend on how much of the forecastle is crushed during the analysis, or in other words how much the nonlinear spring is compressed.

In Section 7.2.5 it is described how the bulb would have to deform 5.27 meters before the forecastle would hit the column, as illustrated in Figure 7.14. It is thus expected that very large collision energies would have to be present for the forecastle to experience significant deformations. What is not accounted for in this assumption, is that as the pontoon is struck by the bulb, the pendulum motion of the pontoon, would bring the pontoon away from the ship. The angle of the column due to this pendulum motion, will thus reduces the crushing depth of the bulb needed before the forecastle would hit the column. This reduction is illustrated in Figure 8.3 and marked with the distance δ

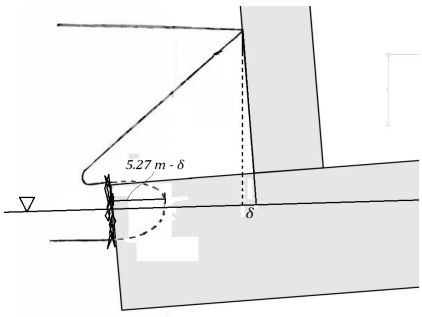

Figure 8.3: Illustration of how the heeling angle of the column, δ affect the crushing depth of the bulb and the forecastle

The total crushing depth of the forecastle would thus be larger than what was expected. In

Figure 8.4 and 8.5 the compression histories of the nonlinear springs representing the forecastle and the bulb respectively, are presented. Would it not have been for the tilt angle and, the distance δ, the total indentation, or compression of both the springs would have been the same. The spring for the forecastle have been compressed 3.17 meter more than the spring for the bulb, setting the value for δ to 3.17 meter.

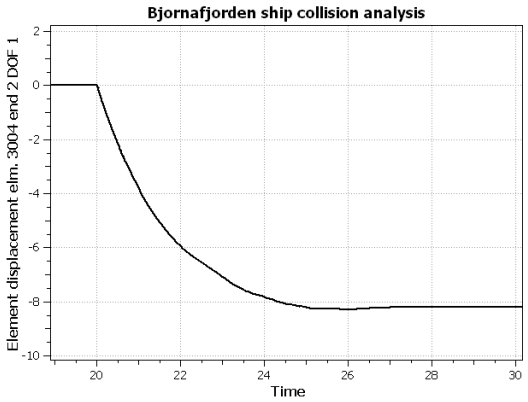

Figure 8.4: Cross section for cable stayed part of bridge. (taken from COWI Report)

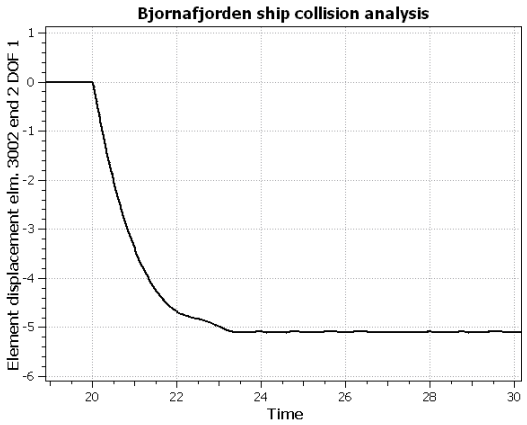

Figure 8.5: Cross section for main part of bridge. (taken from COWI Report)

The compression history for the spring representing the forecastle, given in Figure 8.4, show a maximum compression of 8.27 meters. The first 5.27 meters are as remembered without any stiffness, and before the forecastle hits the pontoons. From the compression history it can thus be found that 3 meters of the forecastle have been crushed in the collision analysis. At this indentation, the width of the ship is smaller than the diameter of the pontoon.

To understand if this interaction could be described well by the local crushing analysis against a rigid wall, a different bow crushing analysis is used as a reference. In this analysis, a ship bow is crushed against a rigid column. The resulting deformation can be seen in Figure 8.6 and 8.7. The exact dimensions of the column and the ship, is not available, but it is seen that the diameter of the column in relation to the width of the bow, is much smaller than what is the case for the ship collisions in collision case 1, which has been discussed above.

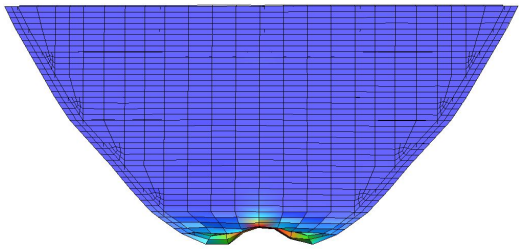

Figure 8.6: Cross section for cable stayed part of bridge (COWI et al. (2016))

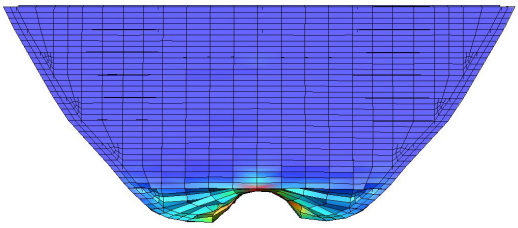

Figure 8.7: Cross section for main part of bridge. (COWI et al. (2016))

What can be noted from the results are that even though the diameter of the column is much smaller than the bow width, the column seems to crush a majority of the bow. Even the steel that is not directly in contact with the column. In Figure 8.6 the width of the ship at the current indentation is approximately twice the diameter of the column, which is much worse than what is experienced in collision scenario 1, where the width of the ship is smaller than 1 diameter

at the maximum indentation. One could thus assume that the whole width of the bow will be crushed when the bow hits the column in collision scenario 1. Using the force-indentation curve for crushing against a rigid wall, might thus not give large errors.

Due to the curved surface of the column, there will however be a delay, where crushing of the steel to the side of the column occur later compared to the steel in front of the column. The steel to the side of the column is only crushed after the column have traveled a distance corresponding to almost 1 column radius into the ship. For crushing against the plane wall, all the steel will be crushed simultaneously over the whole width of the ship. The effect on the force deformation-curve will be that the force on the column will be delayed compared to the force measured on the plane wall, found in the local bow crushing analysis in LS-Dyna.

To account for this, an option could be to shift the force deformation curve used in the analysis, some distance to the right along the x-axis. In this way, the force on a given indentation would be closer to the force-deformation curve one would get from running a bow crushing analysis against the column. This is not done in this thesis, since change in the force-deformation curve, will give only a minor error in the final results. However running a new bow crushing analysis against a column, can be useful if better accuracy are needed in further analyses.

In collision scenario 2, only the pontoon is struck at the long side by the bulb of the ship, and due to the large dimensions of the pontoon, the assumption of a plane wall is a good assumption.

For collision scenario 3, with collision of the forecastle into the bridge girder, the assumption of a plane wall most likely is poor. As can be seen from Figure 8.8, the bridge girders shape is not rounded, making a possibility for it to puncture the ship hull. If this happens, the force-indentation curve of the ship-bridge interaction would differ greatly from the one obtained from the bow crushing analysis against the rigid wall.

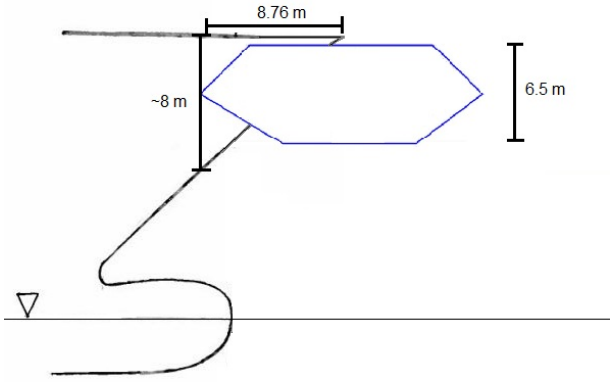

Figure 8.8: Illustration of bridge-ship interaction for collision scenario 3

Additionally, for a collision energy of 450 MJ, it was found that the bridge would crush 8.76 meter of the forecastle. At this indentation, the height of the forecastle is just above 8 meters, while the height of the bridge girder is 6.5 meter, as illustrated by Figure 8.8. This makes it less likely that all the material of the forecastle up to 8.76 meter is crushed. By looking at the Figure it is generally seen that the assumption of a rigid wall, is not a good assumption. It is thus advised to develop a different forc-deformation curve for this collision case to improve the accuracy of the analysis.

8.4.2 Force History of Ship Collision Force

In Section 7.2.3 it is explained how the collision force is introduced through a nonlinear spring, and not as a time dependent force. It was explained how the dynamical response of the structure, could affect the time history of the force. Using the time dependent force, found in a local bow crushing analysis, to represent the collision force is thus not a good The force history found from the local bow crushing analysis against a rigid wall, might thus differ greatly from the time history of the collision force against the responsive bridge. To examine this, the force history of the nonlinear spring elements for each of the collision cases are presented in Figure 8.9 to 8.12.

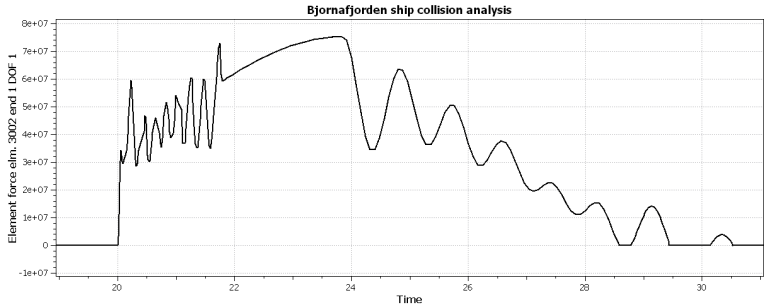

Figure 8.9: Force history of nonlinear spring representing the bulb in collision scenario 2. For a collision energy of 900 MJ

For it to be possible to apply the time dependent force found from the local bow crushing analysis, the compression of the nonlinear spring would have to follow the same steady compression speed as was used in the analysis. No oscillations due to the response of the structure can thus affect the deformation of this spring. The shape of the force history over time, would thus have the same shape as the force-deformation curve.

When looking at the force history from case 2, given in Figure 8.9 it is seen that this seems to be the case for the first 23 seconds, and the shape of the curve is very similar to the force-deformation curve shown in Figure 7.17. For this part of the analysis, the dynamics do not show to be very important, and applying a time-dependent collision force might not give large errors. However, after 23 seconds, 3 seconds after impact, as the forces have set the bridge into motions, the force history is seen to be dependent mostly on how the the structural response cause the spring to contract and extract.

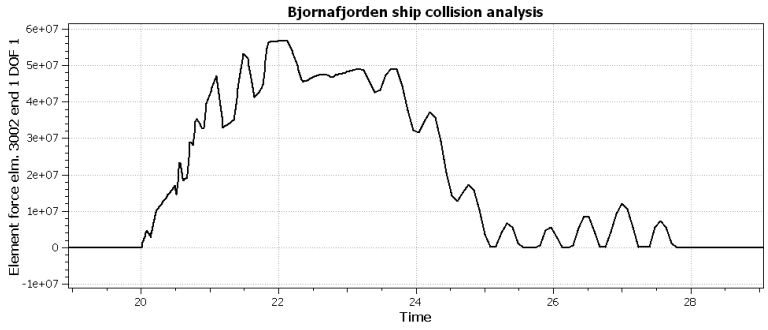

Figure 8.10: Force history of nonlinear spring representing the forecastle in collision scenario 3. For a collision energy of 450 MJ

The same behaviours are observed for the force histories of the springs in the other collision scenarios. The compression of the spring are happening at a constant rate initially, while as the

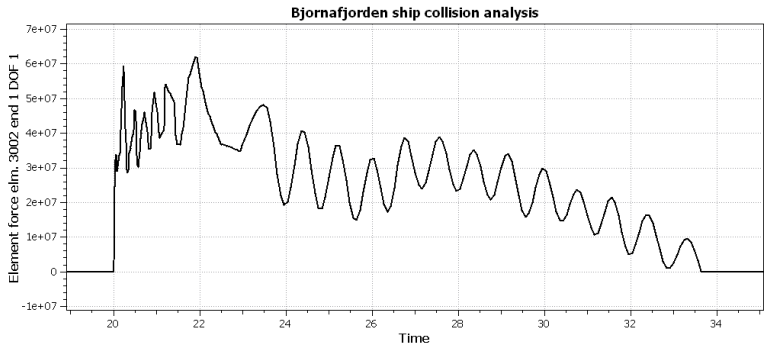

Figure 8.11: Force history of nonlinear spring representing the bulb in collision scenario 1. For a collision energy of 900 MJ

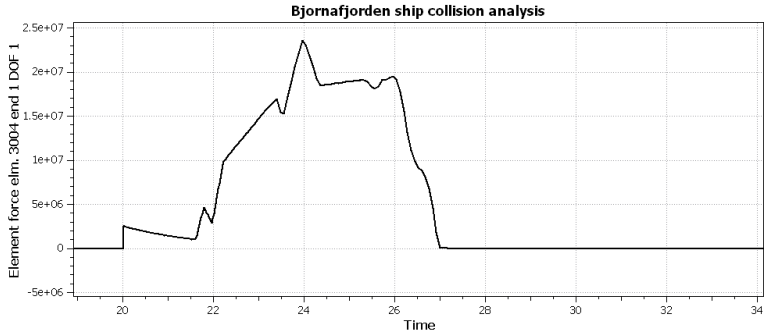

Figure 8.12: Force history of nonlinear spring representing the forecastle in collision scenario 1. For a collision energy of 900 MJ

ship are retarded, the compression rate are depending more and more on the bridges response, thus making the force history's shape deviate more from the shape of the force-deformation curve.

It was found that the most critical stresses are occurring shortly after the impact, and thus up until that time instant, the applied collision force could most likely have been represented fairly correctly by a force history.

The way the force is represented by nonlinear springs in this analysis, is however the preferred method, since it is hard to determine exactly how much the dynamics would affect the force history, before running the analysis. One could also not know if the response of the bridge at later time instances would be critical for the results of the analysis, and these would not be correct when applying the force as a force history instead of a spring.

8.4.3 Position of Impact

A ship impact could occur anywhere along bridge, but analysing all possible scenarios would be impossible within the scope of this Thesis. One should thus try to investigate the scenarios that pose as the biggest threat to the bridge. Collision scenario 1 and 2 are investigated since the probability of an impact are higher and thus it should be able to withstand larger collision energies, as found in Section 7.2.1.

For the rest of the bridge the collision energies are lower, and the collision directly into the bridge girder are checked in collision case 3. It is however not straight forward to say, which

position on the bridge, that would give the worst stresses. A collision closer to the midpoint of the bridge, might be more critical than collision investigated in collision scenario 3. It was however, found that the local bending modes was most critical for the bridge, and these modes would most likely be very similar for all positions along the bridge, and the worst case would be an impact in the middle of two pontoons, as was analyzed.

The main reason why this position was investigated was that at this height, the tip of the bow would crash into the bridge girder. For lower parts of the bridge, where the centerline of the bridge girder is constant at 14.75 meters, the bridge would hit the lower parts of the bow, and thus the force-deformation curve for crushing of the ship bow, would differ greatly from what was found in the local bow-crushing analysis. Even more so than what seen and discussed in Section 8.4.1.

8.4.4 Acceptable Plastic Utilization Factors

Ship collisions are in the Norsok standard characterized as an Accidental limit state(NORSOK STANDARD N-004, Design of steel structures, 2004, page 48). For such scenarios the loading are very extreme, and it is not necessary for the bridge to withstand the loading without being damaged. When looking at ALS loading it is required that "the accidental action does not lead to complete loss of integrity or performance of the structure"(Norsok standard: N-001. Integrity of offshore structures, page 21), but minor damage and the need for repair are accepted.

Minor plastic deformations in the bridge, can thus be tolerated, as long as it doesn't jeopardise the integrity of the structure. The USFOS software are able to calculate the response of the structure, also outside the elastic domain, and experiencing yield in a member of the structure, will thus not necessarily mean that the response are unacceptable. If the structural strength of the structure are intact, and the structure do not risk collapse, a response containing plastic deformations could still be accepted.

However when modeling the structure, several assumptions are made, as previously discussed, and there are significant uncertainties connected to the results obtained. One would thus want to have a safety margin to allow for some errors in the calculations without causing the recommendations for the structure to change.

Exactly how much residual strength the structure would need before collapse are hard to determine. For the analyses in this Master's Thesis, keeping the plastic utilization factor below 1 are seen to be reasonable to use as a guideline. While setting up the analyses, keeping the assumptions conservative are emphasized. The largest collision energies analysed, are also most likely larger than what would be the limit for the ALS criteria. In this way, a plastic utilization below 1 probably would give sufficient confidence to that the structure would survive the loading.

8.4.5 Discussion of Results

In collision scenario 1 the plastic utilization found in the cross beams are fairly high. For the maximum collision energy tested, 900 MJ, the utilization factor was 0.905 and 0.904 for the two beams. This is however below 1, and even with some errors in the modeling, the structure would most likely survive the loading. It is thus not needed to recommend for any strengthening of the structure based in this collision scenario.

For the bridge girder, the plastic utilization was seen to have a maximum increase of 0.586 above the column connection. If this is critical for the structure, will as discussed in Section 3.4, depend on what the utilization would be due to the permanent loading. Should the permanent loads give a utilization factor much higher than 0.5, it is possible that this collision scenario would give large plastic deformations in the bridge girder, with the risk for critical loss of integrity.

The utilization increase close to the cable tower is seen to be 0.116 for the highest collision energy. The initial utilization from the permanent loads thus have to be in the order of 0.9 for this to be critical for the bridge, and this is seen as very unlikely. The same is the case for collision scenario 2 and 3.

Collision scenario 2 gives an utilization increase in the girder above the struck pontoon of 0.656 for the highest collision energy. This level of increase do not give room for very high initial stresses, and with a plastic utilization of only 0.45 initially, this loading will be in the range of what can be critical for the structure. Depending on the real initial plastic utilization, this point on the bridge might have to be strengthened for it to survive the level of loading analyzed.

The results from collision scenario 2, also show a very high plastic utilization at the top of the columns of the struck pontoon. Even for the analysis with the lowest collision energy, 500 MJ, the utilization factor is 0.992, and for the highest energy the utilization factor is 1. As seen in Figure 8.13, the analysis with the highest collision energy gives significant plastic deformations of the column, and after the unloading of the collision force, the columns are seen to have irreversible deformations causing a heel angle of the pontoon. The analysis did not show indication of collapse or for the bridge to loose its weight bearing strength. However, with the amount of uncertainties connected to the results, such large plastic deformations indicates that the strength of the columns may be too low, and must thus be strengthened.

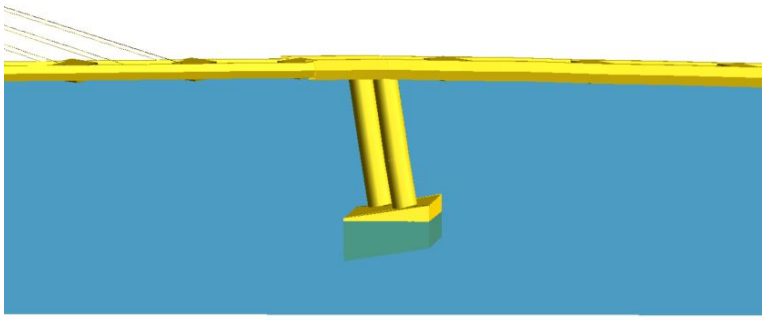

Figure 8.13: Irreversible deformations of the columns due to plastic deformations during ship collision of 900 MJ. Displacements scaled by a factor of 5.)

Since only the upper part of the column, at the connection to the bridge girder, are experiencing these large stresses, it is probably sufficient to only strengthen this part of the column. This can be solved by making the diameter of the upper part of the column gradually increasing towards the connection to the girder, as a coned connection, or increasing the steel thickness as illustrated in Figure 8.14. Introducing significant internal strengthening of the connection is also recommended.

For collision scenario three the collision energies are significantly lower than for the two other collision scenarios, which is seen to affect the stress levels in the results. For the highest

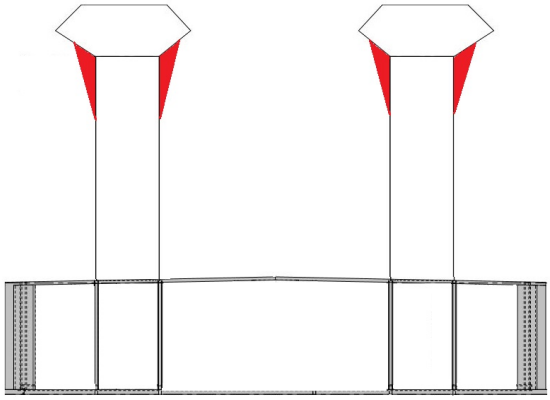

Figure 8.14: Illustration of an example of how to strenghten the upper part of the columns to withstand the bending moments over the connection to the bridge girder

collision energy analyzed, the maximum plastic utilization found is 0.763, which will not be critical for the structure. No strengthening is thus needed due to this collision scenario.

8.4.6 Displacements and Accelerations

The most extreme displacements and accelerations of the bridge girders are also determined in the analysis. This is because these values might be critical in ways that are not clear from the structural analysis. Large accelerations might for example impacts on the traffic on the bridge, causing loss of life due to multi-vehicle-collisions. This can be due to the asphalt being destroyed as is seen in earthquakes, or due to loss of traction and steering.

For collision case 3 it is noted that the horizontal accelerations found are extremely high. This can probably be explained by the fact that due to the use of few nodes in USFOS, the accelerations were measured in the same node as the collision force were applied. The accelerations might thus not be very realistic as values for the accelerations experienced at the traffic lanes. However it can be noted that since the ship will hit directly into the pathways, large accelerations can occur, which can be a problem for the traffic.

Discussions around this could be made, saying that it should be assumed that the drivers would see the ship before impact, and avoid during at the point of impact. However, this discussion is not relevant to the Master thesis, and will not be investigated further.

8.4.7 Local Damage

In this thesis, the focus is on the global response of the structure when subjected to ship collisions. Local damage caused by the collision have thus not been investigated. A strength design is assumed when running the analysis, which assumes a neglectable amount of local deformations of the bridge during the collision. When the ship is striking the bridge, it is however a chance that the local strength of the bridge is too low for it to withstand the impact. The bulb might puncture the hull of the pontoon, or the forecastle might cause local buckling in the columns. This may cause critical damage to the structure that are not accounted for in this analysis. To be able to comment on the local response on the structure when subjected to the ship collision, local analyses would have to be conducted. For this purpose the USFOS model would

not be appropriate, and different model would have to be developed using another software.

The effect of local damage on the global strength could be investigated very roughly in the global analysis by assuming total failure of the damaged elements. For example a local buckling of the the column after being struck by the ship, could be simulated by removing the element during the analysis, after the collision forces have been transferred into the bridge. The forces would then have to be redistributed to other parts of the structure, which could have a large effect on the results of the collision analysis, and might cause a critical loss of strength for the structure.

A puncture of the pontoons could be introduced by gradually filling the pontoon with water after the impact of the bulbous bow. How this would affect the global strength during the collision analysis, could thus be checked. Since the pontoons had several watertight departments, the amount of water entering the pontoon would not be large, and the effect is thus not expected to be very large, but could maybe affect the result somewhat.

As discussed in the preface, these analyses where not completed, due to the amount of extra work improving the model. This is therefore suggested as a suggestion for further work.

Chapter 9

Conclusion

The investigations performed in this thesis are part of the preliminary studies for developing a strait crossing design for Bjørnafjorden. Because the project is still in the early phase of development, exact details for the design are not given and significant uncertainties are connected with the work. Conclusion to whether the bridge would survive the ship collisions could thus never be a hundred percent certain, and should be seen in connection with the discussions presented in Chapter 8.

In the analysis of collision scenario 1, where the ship hits the short end of the pontoon closest to the navigational channel the maximum plastic utilization occur in critical point number 3, which is in the third cross-beam to the north away from the struck pontoon. The plastic utilization factor was 0.905 for the maximum collision energy of 900 MJ. For assessment of the bridge girder, the increase in the plastic utilization factor is investigated, due to difficulties in modeling the pre-tension in the cable wires for the cable stayed section, as is discussed in Section 3.4. The maximum increase is found at critical point 1, at where the rearmost column is connected to the bridge girder. The increase was found to be 0.486, and as long as the utilization caused by the initial stresses are below 0.5, the bridge would not need to be strengthened for this collision scenario.

From the analyses of collision scenario 2, where the pontoon closest to the navigational channel is struck in the transverse direction, very high plastic utilization factors were observed in the column of the struck pontoon. At the top of the column, in the connection to the bridge girder, in what is defined as critical point 1, the plastic utilization factor was found to be 0.992 for the lowest collision energy investigated of 500MJ. For the maximum collision energy of 900 MJ, large plastic deformations are observed, and it is thus advised to strengthen the upper part of the pontoon columns.

In collision scenario 3, the plastic utilization factors observed, are low, with a maximum value of 0.763 in one of the cross beams. The global strength of the bridge thus seem to be sufficient for collision like this, into the bridge girder, and no strengthening are advised. The collision energies used for this collision scenario are much lower than for collision scenario one and two, with a maximum value of 450 MJ. This is a result of it being further away from the navigational channel, and thus was found to be less prone to collisions in the analysis performed by the SSPA.

Chapter 10

Further Work

Point five and six of the scope of work was not finished during the time available for the thesis work. These will thus be suggested for further work. A residual strength analysis could be developed to look at the global strength of the structure after experiencing loss of strength due to local damage. A first approach could be to look at the effect of a buckled pontoon column, or a pontoon filled with seawater due to a puncture of the pontoon hull. Reduced strength of the bridge girder could also be assessed due to local damage from impact from the ship forecastle.

The work of analysing the bridge with relation to wave and wind forces, as described in point five of the scope of work, will be very important for the bridge design. Extensive investigations should thus be done to determine the bridges response to such loading.

Point number four from the scope of work, was not possible to perform, because the work done with developing the software for non-central impacts in USFOS were not finished. This is currently under development, and when finished, it should be used to investigate such collision cases.

From the damping analyses, it is found that the change in damping had only minor effect on the results for the ship collision scenarios analyzed. However as discussed, the damping level would affect other investigations, like for environmental loading as an example. It is thus advised to develop a more exact estimation for the damping levels used when analyzing the bridge.

In Section 8.4.1 it is discussed how the force-indentation curve used to represent the local ship-bridge interaction, may be a poor approximation, especially for impacts with the bridge girder. Running local bow crushing analyses against different parts of the bridge are thus advised to determine how this curve will differ for the different geometries of the bridge. How much a change in the force-indentation curve will affect the final results of the global ship collision analysis, was not investigated in this Thesis. It is advised to do an assessment of this, the work with developing new force deformation curves are done, in case the improvement is found to, be small and not worth the extra work.

Local analyses should be performed to asses the local strength of the bridge. Only the global strength have been investigated in this Thesis, where the local strength have been assumed sufficient to withstand the collision force. These assumptions could be wrong, and extensive work should be done to check the local damage due to ship impacts. A first approach could be to check the risk of the bulb of the ship puncturing the pontoon, or the forecastle causing a local buckling of the pontoon columns.

Further work should be done to determine what requirements should be set for the maximum accelerations of the bridge. If such requirements are found, a more extensive investigation of the response should be done to check for critical accelerations. The accelerations in some points on the bridge are presented in this Thesis, but more extensive investigations could on this matter.

Bibliography

[1] O. M. Faltinsen *Sea Loads on Ships and Offshore Structures*, 1999.

[2] Carl M. Larsen. *TMR4182 - Marine Dynamics*, 2014.

[3] Ivar Langen and Ragnar Sigbjørnsson. *Dynamisk Analyse av konstruksjoner*, 2007.

[4] Yanyan Sha and Jørgen Amdahl. *Design of Floating Bridge Pontoon subjected to Ship Collision Load*, 2016.

[5] COWI, Aas-Jakobsen, Johs Holt AS and Global Maritime. *Curved Bridge – Navigational Channel in South*, 2016.

[6] COWI, Aas-Jakobsen and Johs Holt AS. *Bridge Drawings, South Navigational Span, Curved Bridge*, 2015.

[7] Jørgen Amdahl and Ernst Eberg. *Ship collision with offshore structures*, 1993.

[8] Olav Furnes and Jørgen Amdahl. *Ship collision with offshore platforms*, 1993.

[9] Statens Vegvesen. *Multi-span suspension bridge on floating foundations - E39 Bjørnafjorden*, 2015

[10] European Comittee For Standarisation. *Eurocode 1 - Actions on structures - Part 1-7: General actions - Accidental actions*, 2006 (1991)

[11] European Comittee For Standarisation. *Eurocode 1, PART 1.7 - Accidental Actions - Background Document*, 2005

[12] DNV. *Recomended Practice - DNV-RP-C205 - Environmental Conditions and Environmental Loads*, 2007

[13] Am. Assoc. of State Hwy.and Transp. Officials, *AASHTO Guide specification*, 2009

[14] L.H. Bjøndal, M.J. Akhtar, B. Forsman, A. Andersson, E. Wilske. *Ship collision for risk analysis for the planned crossing if bjørnafjorden*, 2016a

[15] L.H. Bjøndal, M.J. Akhtar, B. Forsman, A. Andersson, E. Wilske. *The choice of multiple design ships for calculation of bridge collision design loads*, 2016b

[16] A. Andersson, E. Wilske, B. Forsman. *Risk assesment of bridge collision - using Monte Carlo Simulation*, 2015

[17] Ole Harald Moe. *Master Thesis - Analysis and Design of Bjørnafjorden TLP Supported Suspension Bridge Subjected to Large Ship Collisions and Extreme Environmental Loads*, 2016

[18] Jørgen Lima Hansen. *Master Thesis - Analysis and Design of Ship Collision Barriers on a Submerged Floating Tunnel subjected to Large Ship Collisions*, 2015

[19] Ørjan Konstali. *Master Thesis - Analysis and Design of Ship Collision Barriers on a Submerged Floating Tunnel subjected to Large Ship Collisions* , 2014

[20] Marintek. *Usfos getting started. SINTEF GROUP*, 2001, June

[21] Negrut, D., Ottarsson, G., Rampalli, R. and Sajdak, A. *On an Implementation of the Hilber-Hughes-Taylor Method in the Context of Index 3 Differential-Algebraic Equations of Multibody Dynamics (DETC2005-85096)*, 2006

[22] Sighard F. Hoerner. *Fluid-Dynamics Drag*, 1965

[23] SIEMENS. *Basic Dynamic Analysis User's Guide*, 2014

[24] USFOS Commands Users Manual [Internet]
http://usfos.no/manuals/usfos/users/documents/Usfos_UM_06.pdf

[25] Usfos Example Collection [Website]
http://usfos.no

[26] Reknestykka om Hordfast sprikar i alle retningar [internet]
https://www.nrk.no/hordaland/ekspertane-kranglar-om-kor-nyttig-hordfas

[27] Ferjefri E39 vil gi større verdiskapning enn antatt [internet]
https://www.nrk.no/mr/overrakte-e39-rapport-1.10939292

[28] COWI, obtained through Professor Jørgen Amdahl. Bridge drawings

[29] MS Color Magic 1/2/2017 [internet]
https://en.wikipedia.org/wiki/MS_Color_Magic

[30] Presentation - Floating bridge E39 Bjørnafjorden. (Further edits done by Kirsti Skogseth) 1/2/2017 [Illustration]
http://www.vegvesen.no/_attachment/1545428/binary
/1135143?fast_title=14+Flytebru.pdf

10.1 Appendix: water-plane stiffness of buoyancy elements

When trying to run the dynamic analysis to balance the weight with the buoyancy, the analysis kept crashing. First this was expected to be because the unbalance was too large. A lot of changes were done to try to compensate for this, like temporarily increasing the strength of the bridges cross-sections. After weeks of trial and error Tore Holmås suggested that the water-plane stiffness of the pontoons might be missing.

This was thus investigated for one pontoon, by modeling a buoyancy element with only a spring to ground as the boundary condition was modeled. By applying a moment in pitch, the rotation angle can be anticipated as seen in Figure 10.1 if the only the rotational stiffness from the spring are contributing to the righting moment. If the rotation angle found in the analysis is equal to the one anticipated, one would know that the buoyancy elements does not contribute to the water-plane stiffness in pitch.

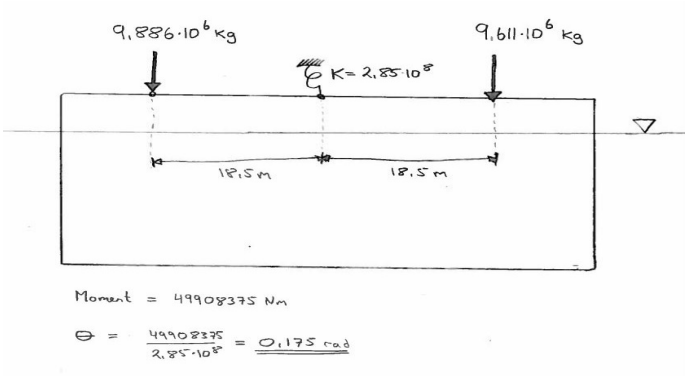

Figure 10.1: Calculating pitch angle

As seen below the, pitch angle seen in Figure 10.2 is the same as anticipated by just the spring stiffness, and thus it is seen that the buoyancy element in itself has no rotational stiffness from the water-plane. This was not known when modeling the bridge, and thus caused a large error in the modeling which was the reason of the analysis crashing.

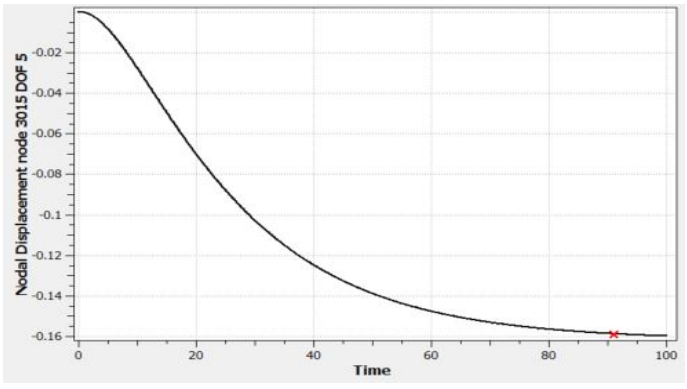

Figure 10.2: Pitch angle of single pontoon, when exposed to a pitch moment

To compensate for this a spring to ground is introduced, with stiffness in roll and pitch as the water-plane stiffness found in the report, and zero stiffness in the other degrees of freedom. In this way the water-plane stiffness is modeled correctly.

10.2 Appendix: Eigenvalue analysis

10.2.1 Eigenmodes from USFOS analysis

Figure 10.3: Eigenmode with eigenperiod of 11.87 seconds

Figure 10.4: Eigenmode with eigenperiod of 11.80 seconds

Figure 10.5: Eigenmode with eigenperiod of 11.71 seconds

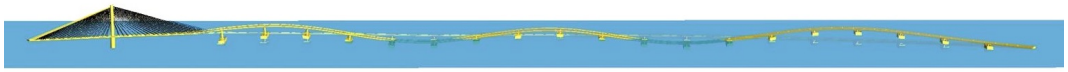

Figure 10.6: Eigenmode with eigenperiod of 11.59 seconds

Figure 10.7: Eigenmode with eigenperiod of 11.44 seconds

Figure 10.8: Eigenmode with eigenperiod of 11.21 seconds

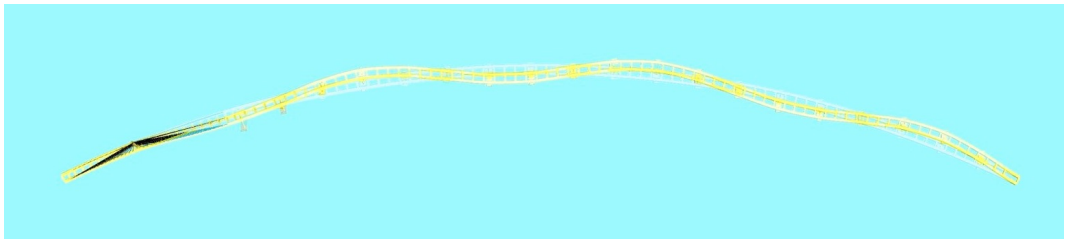

Figure 10.9: Eigenmode with eigenperiod of 11.02 seconds

Figure 10.10: Eigenmode with eigenperiod of 10.87 seconds

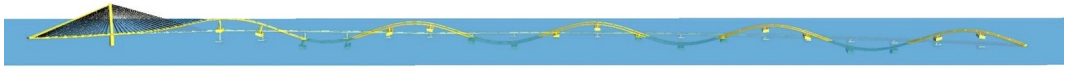

Figure 10.11: Eigenmode with eigenperiod of 10.43 seconds

Figure 10.12: Eigenmode with eigenperiod of 10.25 seconds

10.2.2 Orcaflex

Mode	Period	Frequenzy	X	Y	Z	RX	RY	RZ	Dominating
	[s]	[Hz]	[%]	[%]	[%]	[%]	[%]	[%]	motion
1	56.72	0.0176	18	82	0	0	0	0	Y
2	31.69	0.0316	6	94	0	0	0	0	Y
3	22.68	0.0441	6	81	0	12	0	0	Y
4	18.62	0.0537	11	82	0	6	0	0	Y
5	14.33	0.0698	12	74	0	13	1	0	Y
6	11.90	0.0840	9	20	1	68	1	0	RX
7	11.48	0.0871	10	16	27	45	1	0	RX
8	11.48	0.0871	14	9	49	26	1	0	Z
9	11.02	0.0908	3	0	95	1	0	0	Z
10	10.95	0.0913	0	0	99	0	0	0	Z
11	10.95	0.0913	0	0	99	0	0	0	Z
12	10.94	0.0914	0	0	100	0	0	0	Z
13	10.92	0.0916	0	0	98	1	0	0	Z
14	10.89	0.0918	1	5	89	4	0	0	Z
15	10.81	0.0925	3	2	93	1	1	0	Z
16	10.71	0.0934	4	24	62	9	1	0	Z
17	10.64	0.0940	5	31	51	12	1	0	Z
18	10.48	0.0955	4	0	94	0	1	0	Z
19	10.21	0.0980	5	0	94	0	1	0	Z
20	9.88	0.1012	5	1	93	1	1	0	Z

Figure 10.13: List of eigenvalues given in COWI et al.(2016)

Figure 10.14: Eigenmode 1 from orcaflex given in COWI et al.(2016)

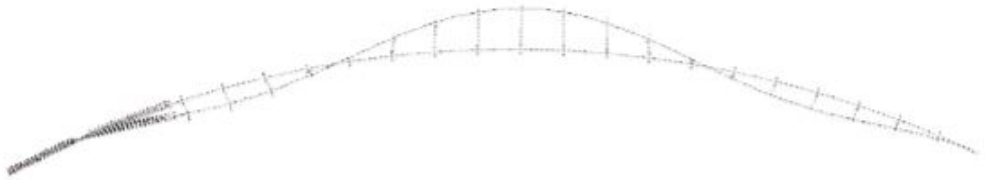

Figure 10.15: Eigenmode 2 from orcaflex given in COWI et al.(2016)

Figure 10.16: Eigenmode 3 from orcaflex given in COWI et al.(2016)

Figure 10.17: Eigenmode 4 from orcaflex given in COWI et al.(2016)

Figure 10.18: Eigenmode 5 from orcaflex given in COWI et al.(2016)

Figure 10.19: Eigenmode 6 from orcaflex given in COWI et al.(2016)